Author Manuscript

Author Manuscript

Author Manuscript

Author Manuscript

HHS Public Access

Author manuscript

Cell Rep. Author manuscript; available in PMC 2020 January 31.

Published in final edited form as:

Cell Rep. 2020 January 14; 30(2): 351–366.e7. doi:10.1016/j.celrep.2019.12.027.

T-bet+ Memory B Cells Link to Local Cross-Reactive IgG upon Human Rhinovirus Infection

Jacob D. Eccles[1], **Ronald B. Turner**[2], **Nicole A. Kirk**[1], **Lyndsey M. Muehling**[1], **Larry Borish**[1], **John W. Steinke**[1], **Spencer C. Payne**[1,3], **Paul W. Wright**[1], **Deborah Thacker**[2], **Sampo J. Lahtinen**[4], **Markus J. Lehtinen**[4], **Peter W. Heymann**[2], **Judith A. Woodfolk**[1,5,*]

[1]Department of Medicine, University of Virginia School of Medicine, Charlottesville, VA 22908, USA [2]Department of Pediatrics, University of Virginia School of Medicine, Charlottesville, VA 22908, USA [3]Department of Otolaryngology, University of Virginia School of Medicine, Charlottesville, VA 22908, USA [4]DuPont Nutrition & Biosciences, Global Health and Nutrition Science, Sokeritehtaantie 20, 02460 Kantvik, Finland [5]Lead Contact

SUMMARY

Human rhinoviruses cause the common cold and exacerbate chronic respiratory diseases. Although infection elicits neutralizing antibodies, these do not persist or cross-protect across multiple rhinovirus strains. To analyze rhinovirus-specific B cell responses in humans, we developed techniques using intact RV-A16 and RV-A39 for high-throughput high-dimensional single-cell analysis, with parallel assessment of antibody isotypes in an experimental infection model. Our approach identified T-bet+ B cells binding both viruses that account for ~5% of CXCR5− memory B cells. These B cells infiltrate nasal tissue and expand in the blood after infection. Their rapid secretion of heterotypic immunoglobulin G (IgG) *in vitro,* but not IgA, matches the nasal antibody profile post-infection. By contrast, CXCR5+ memory B cells binding a single virus are clonally distinct, absent in nasal tissue, and secrete homotypic IgG and IgA, mirroring the systemic response. Temporal and spatial functions of dichotomous memory B cells might explain the ability to resolve infection while rendering the host susceptible to re-infection.

In Brief

This is an open access article under the CC BY-NC-ND license (http://creativecommons.org/licenses/by-nc-nd/4.0/).

*Correspondence: jaw4m@virginia.edu.

AUTHOR CONTRIBUTIONS

J.D.E., R.B.T., L.M.M., L.B., J.W.S., P.W.H., S.J.L., M.J.L., and J.A.W. designed the experimental challenge models. J.D.E. performed all experiments except for neutralizing assays. N.A.K. prepared virus for cell labeling and antibody assays. D.T. performed neutralizing assays. R.B.T. and P.W.H. contributed serum and nasal wash samples. L.B., S.C.P., and J.W.S. contributed biopsy samples. L.M.M. provided intellectual input on all aspects of the study. P.W.W. and L.M.M. prepared specimens, provided logistical support for virus challenge studies, and generated databases. J.D.E. and J.A.W. analyzed the data and drafted and finalized the manuscript. All authors assisted with manuscript preparation.

DECLARATION OF INTERESTS

J.D.E., R.B.T., L.M.M., J.A.W., L.B., P.W.H., and J.W.S. received research funding or salary support from the sponsors for the conduct of this study. At the time of RV challenge, S.J.L. and M.J.L. were employees of DuPont Nutrition and Health, which sponsored the RV-A39 challenge studies. All other authors declare no competing interests.

SUPPLEMENTAL INFORMATION

Supplemental Information can be found online at https://doi.org/10.1016/j.celrep.2019.12.027.

Author Manuscript Author Manuscript Author Manuscript Author Manuscript

Eccles et al. demonstrate a key role for T-bet+ B cells in rapid local cross-reactive immunoglobulin G (IgG) responses to rhinovirus, whereas strain-specific B cells that are phenotypically distinct match systemic antibodies found later. This might explain efficient clearance of virus in the acute phase but narrow protection and continued susceptibility after the infection clears.

Graphical Abstract

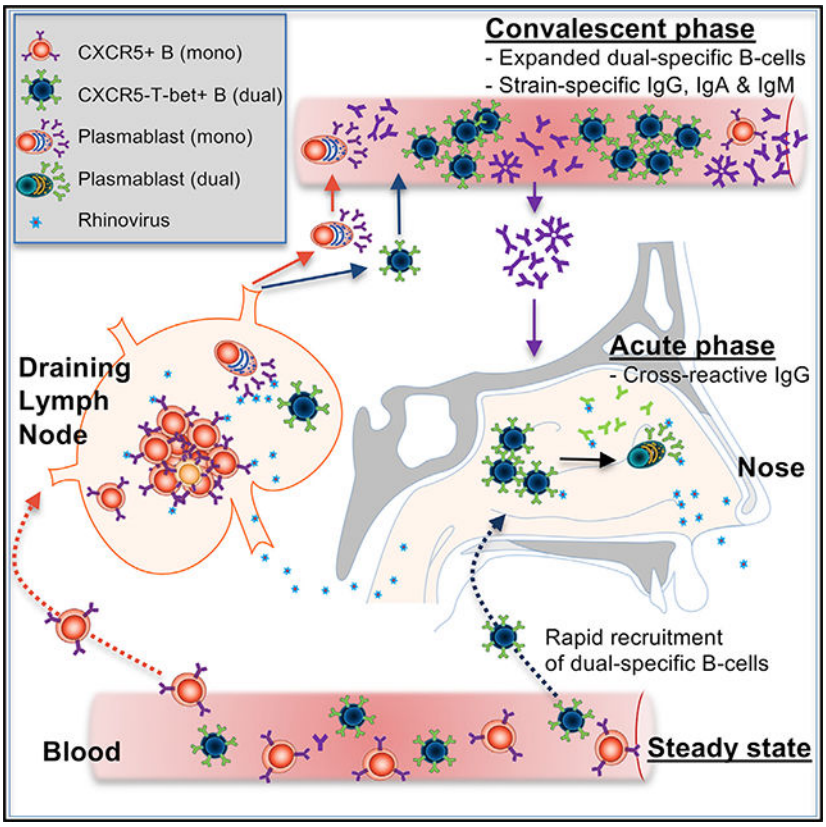

INTRODUCTION

Rhinovirus (RV) is a major cause of the common cold. This disease presents an enormous health and economic burden based on the high infection rates in the general population and its exacerbation of chronic respiratory disorders in infected patients (Bertino, 2002; Calhoun et al., 1994; Fendrick et al., 2003; Iwane et al., 2011; Nichol et al., 2005; Roelen et al., 2011). It has long been known that infection induces the production of neutralizing antibodies; however, these antibodies wane after several months and do not appear to cross-protect against multiple RV strains (Barclay et al., 1989; Fleet et al., 1965; Glanville and Johnston, 2015). This latter feature has been attributed, at least in part, to the antigenic variability across the more than 160 serotypes of RV, which are responsible for an estimated 6–10 infections per year in children (Hendley, 1998; Jacobs et al., 2013; Turner, 2007). Despite over four decades of study on antibody responses to RV in infected humans, nothing is known about the nature of RV-specific B cells in humans. Thus, advancing knowledge in

Author Manuscript Author Manuscript Author Manuscript Author Manuscript

this area could yield new insight into the humoral response to RV and, more specifically, the attributes of B cell memory to one of the most ubiquitous viral pathogens in humans.

Recent work has implicated human B cells that express T-bet in anti-viral responses (Chang et al., 2017; Knox et al., 2017). Although originally defined as a lineage-specifying transcription factor for Th1 cells, T-bet regulates anti-viral B cell responses in mouse models, and is pivotal to B cell differentiation and isotype switching, as well as expression of interferon-γ (IFN-γ) and the chemokine receptor CXCR3 in B cells (Barnett et al., 2016; Kallies and Good-Jacobson, 2017; Lazarevic et al., 2013; Lebrun et al., 2015; Piovesan et al., 2017; Rubtsova et al., 2013; Rubtsova et al., 2017). T-bet+ B cells, which represent 0.1% −2% of total B cells, accumulate over the lives of humans and mice, and accordingly have been termed “age-associated B cells” (ABCs) (Hao et al., 2011; Manni et al., 2018; Rubtsov et al., 2011). These cells are also elevated in the circulation of patients with chronic viral infections and autoimmune diseases, consistent with their antigen-driven expansion (Chang et al., 2017; Jenks et al., 2018; Knox et al., 2017; Wang et al., 2018). Although their specificity remains largely unknown, this phenotype was recently found to comprise the majority of B cells specific for gp140 in chronically infected HIV-positive individuals (Knox et al., 2017). Consistent with the notion of a primary role in anti-viral immunity, selective knockout of T-bet in B cells results in severe immune deficiency in a viral infection model (Barnett et al., 2016). Despite this knowledge, the signature of class-switched T-bet+ B cells reported in the literature varies depending on the markers analyzed across different studies; however, predominant expression of the IgG isotype, and expression of the myeloid marker CD11c, are notable features (Karnell et al., 2017). By contrast, expression of memory B cell markers such as the B cell co-receptors CD21 and CD27, is not prominent (Lau et al., 2017; Li et al., 2016). This latter feature is akin to “tissue-like” memory B cells found in the blood of patients with HIV viremia, which were so described based on their resemblance to memory B cells in tonsillar tissue (Ehrhardt et al., 2005; Moir et al., 2008).

We theorized that the high number of infections with RV in humans might favor outgrowth of virus-specific B cells with attributes similar to T-bet+ B cells but that lack cross-reactive function. To address this, we performed the first comprehensive longitudinal analysis of human RV-specific B cells in parallel with anti-viral antibody isotypes, both in steady state and during experimental infection, using two different RV-A strains. Virus-specific B cells were detected using whole virus, in conjunction with a high-dimensional method in order to detect subtle variations in rare B cell types. By this approach, virus-specific memory B cells were found to display two distinct signatures based on differential expression of the chemokine receptor CXCR5. Surprisingly, CXCR5- memory B cells were dual specific according to labeling with both RV-A strains tested, expressed T-bet, and rapidly secreted cross-reactive IgG, but not IgA or IgM. Moreover, these cells expanded in the blood after infection, and tissue-infiltrating dual-specific T-bet+ B cells present in the nose during the acute phase coincided with local rapid secretion of cross-reactive IgG. By contrast, CXCR5+ virus-specific B cells were mono-specific and secreted strain-specific isotypes matching those antibodies found later in the nose and serum.

Our findings demonstrate a pivotal role for cross-reactive T-bet+ memory B cells in the response to different RV-A strains, and establish distinct spatial and temporal effector

Author Manuscript Author Manuscript Author Manuscript Author Manuscript

functions for discrete B cell types that enable efficient clearance of different rhinoviruses acutely, but narrow protection and continued susceptibility after infection.

RESULTS

Whole Virus Detects Multiple RV-Specific Isotypes

High levels of antibodies to capsid protein subunits of RV species have been reported in human serum (Ding et al., 2018; Megremis et al., 2018; Niespodziana et al., 2012), even when infection is not detected (Iwasaki et al., 2014). Thus, the biological relevance of such antibodies is unclear. We posited that whole virus is best suited to label RV-specific antibodies and identify virus-specific B cells, since it contains native epitopes formed by the four capsid proteins integral to the icosahedral capsid structure. To this end, two distantly related strains of the RV-A species, RV-A16 and RV-A39 (76% genome identity, 80% capsid protein identity), were propagated in culture. Their structure and durability were verified by electron microscopy (Figure 1A), their identities were confirmed by RT-PCR (Figure 1B) and purity was assessed by SDS-PAGE analysis and western blot against the capsid protein VP2 (Figure 1C). Next, both viruses were incorporated into a novel bead-based multiplex assay to simultaneously monitor changes in serum antibodies specific for both RV-A strains in subjects who were experimentally infected with either RV-A16 or RV-A39 (Figure 1D). By this method, increases in IgG, IgA, and IgM specific for the infecting strain (i.e., homotypic antibodies) were detected in the serum, 21 days after experimental infection (IgG, $p < 0.0001$; IgA, $p < 0.0001$; IgM, $p < 0.01$) (Figure 1E). However, increases in antibodies to the heterotypic RV strain were not detected, with the exception of a modest rise in IgG ($p < 0.01$). As expected, serum antibodies were unchanged in subjects who did not become infected (Figure S1), and no change was observed for serum antibodies to negative (mouse IgG) and positive (tetanus toxin C-terminal fragment) control antigens (Figure 1E). Notably, serum antibodies to the capsid subunit, VP1, did not change after infection, indicating a lack of specificity for virus (Figure 1F). These findings validated whole virus as a biologically relevant target, and confirmed that IgG, IgA, and IgM antibodies induced by RV infection in the serum are predominantly strain specific.

Dual-Specific B Cells Are Expanded in the Blood and Lack CXCR5

Next, to identify RV-specific B cells, virus was tagged with fluorophore and integrated into a B cell surface-staining antibody panel for multi-color flow cytometry. B cells were first analyzed in the blood of healthy uninfected subjects based on the premise that virus-specific memory B cells would be detectable as a result of previous RV exposures. We elected to analyze RV-specific B cells in the context of CXCR5, a chemokine receptor that is critical to the retention of B cells within follicles of secondary lymphoid organs. We posited that the lack of expression of this marker might delineate those virus-specific B cells with a tissue homing predilection capable of secreting antibodies at the infection site. This was based on the following: (1) low expression of CXCR5 on antibody-secreting plasma cells, which facilitates their egress from lymphoid organs (Dullaers et al., 2009; Hargreaves et al., 2001); and (2) previous reports of CXCR5lo/− B cells with a tissue-like phenotype in chronic viral infections (Moir et al., 2008; Portugal et al., 2015; Weiss et al., 2009). Staining of peripheral blood mononuclear cells (PBMCs) with whole virus revealed that RV-specific B cells were

Author Manuscript Author Manuscript Author Manuscript Author Manuscript

predominantly IgD-negative (i.e., class switched) memory cells and enriched for CXCR5− cells (~30% of RV-specific B cells versus < 3% of total memory B cells) that expressed higher levels of CD20 compared with their CXCR5+ counterparts (Figures 2A and 2B). Analysis of total B cells revealed CXCR5− cells that labeled with both RV-A16 and RV-A39, whereas cells that labeled with only a single virus were enriched for CXCR5+ cells (Figure 2C). This unexpected finding demonstrated the presence of CXCR5− dual-specific and CXCR5+ mono-specific B cell types. Within memory B cells, the numbers of CXCR5+ cells are typically >20-fold higher than CXCR5− cells. Despite this, calculation of the absolute percentages of mono-specific and dual-specific cells within memory B cells confirmed that CXCR5− dual-specific cells constituted a high percentage (up to 3%) of memory B cells (Figure 2D). Moreover, this phenotype was the most abundant memory with RV specificity within the B cell compartment (0.09% ± 0.05%) (Figure 2E). Upon further inspection, 75.2% ± 10.5% of dual-specific B cells were CXCR5−, versus 23.7% ± 15.6% of mono-specific B cells (Figure 2F), while only 3.3% ± 0.8% of total memory B cells were CXCR5−. Moreover, RV-specific B cells (mono-specific + dual-specific) comprised 5.0% ± 2.7% of total CXCR5− memory B cells, and dual-specific B cells were the dominant subset (3.8% ± 2.0%) (Figure 2G). Given that the frequency of B cells with a given specificity is typically less than 0.1% of total B cells (Doria-Rose et al., 2009; Franz et al., 2011; Lanzavecchia et al., 1983), the relative abundance of dual-specific memory B cells within the CXCR5− subset was striking and likely reflected expansion from previous RV infections.

To ensure that labeling of B cells by virus was occurring via surface B cell receptor (BCR), and not via the major RV receptor ICAM-1, our staining method incorporated an excess of anti-ICAM-1 antibody. However, even when ICAM-1 blocking was omitted, a lack of correlation between virus binding and ICAM-1 staining indicated that binding of virus to B cells by surface ICAM-1 was not a feature (Figure 2H).

Next, to probe the possible functional relevance of a lack of CXCR5 expression on dual-specific B cells, we compared the phenotype of CXCR5− and CXCR5+ cells within total memory B cells. Those memory B cells that lacked CXCR5 were found to express higher levels of the transcription factor T-bet (~60% T-bet+), as well as the myeloid marker CD11c, and the Th1-associated receptors, CCR5 and CXCR3, whose ligands are induced in the nose during acute RV infection (Figures 2I, 2J, and 2K) (Muehling et al., 2018). Moreover, CXCR5− memory B cells were enriched for the IgG isotype compared with their CXCR5+counterpart (Figure 2K). Thus, CXCR5− memory B cells fit the signature of T-bet+ B cells reported in chronic viral infections (Chang et al., 2017; Knox et al., 2017). Given that CXCR5 contributes to B cell homing to, and navigation within, lymphoid tissues (Breitfeld et al., 2000; Okada et al., 2002), its absence on dual-specific B cells, coupled with higher levels of CCR5 and CXCR3 on CXCR5− memory B cells, might favor migration of dual-specific B cells to the tissues, analogous to those tissue-like B cells implicated in chronic viral infections (Moir et al., 2008; Portugal et al., 2015; Weiss et al., 2009).

Author Manuscript Author Manuscript Author Manuscript Author Manuscript

Dual-Specific B Cells Rapidly Secrete Cross-Reactive IgG but Not IgA or IgM

Next, to test for effector function, the capacity for dual-specific B cells to secrete cross-reactive antibodies was assessed by culturing under conditions that differentiate plasma cells (Karahan et al., 2014). Cells were isolated to high purity by fluorescence-activated cell sorting to compare the function of B cells with dual-specificity versus mono-specificity. To accomplish this, B cells were first gated for binding of RV-A16 only, RV-A39 only, or both viruses. The remaining non-specific cells were gated into naive, CXCR5+ memory, and CXCR5− memory B cell types, to give a total of six sorted B cell populations. Culture supernatants were collected every 2 days for antibody analysis. Dual-specific B cells predominantly secreted IgG antibodies that were cross-reactive for RV-A16 and RV-A39, while secretion of other RV-specific isotypes was minimal. The predominance of IgG was also a feature of non-specific CXCR5− memory B cells. By contrast, mono-specific B cells secreted strain-specific IgG, IgA, and IgM antibodies, echoing the isotype profile of non-specific CXCR5+ memory B cells (Figures 2K and 3). Dual-specific B cells responded more rapidly than their mono-specific counterpart, based on the detection of IgG as early as day 2 in culture. In addition, non-specific CXCR5− memory B cells differentiated more rapidly than non-specific CXCR5+ memory B cells under plasmablast differentiating conditions, as judged by upregulation of CD27 and downregulation of CD20 (Figure S2).

Weak signals for cross-reactivity were detected for mono-specific B cells, but for IgG only (Figure 3, top left). This likely arose from contamination with dual-specific B cells. Non-specific CXCR5+ and CXCR5− memory B cell subsets also gave signals for anti-RV IgG and IgA (CXCR5+) or anti-RV IgG only (CXCR5−), indicating the presence of residual RV-specific B cells within these more abundant subsets. As expected, these B cell types also secreted tetanus-specific antibodies. Taken together, these findings established the ability for dual-specific memory B cells to rapidly secrete cross-reactive IgG and distinguished their specificity and antibody profile from mono-specific B cells.

High-Dimensional Analysis Reveals a Characteristic Signature of Dual-Specific B Cells

Our next step was to rigorously interrogate the molecular signature of dual-specific B cells and test their ability to respond to *in vivo* infection. To accomplish this, mass cytometry was applied to our experimental infection model. To ensure the sensitive and reliable detection of alterations in B cell types during infection, including rare RV-specific cells, PBMC samples that were enriched for B cells, were barcoded by a novel method that combined anti-CD45 and anti-MHCI antibodies labeled with eight different metal isotopes. Samples were then pooled for mass cytometry analysis. This allowed all samples to be prepared under identical conditions and run in a single experiment, thereby minimizing batch effects that might obscure changes in rare B cell subtypes. Seventy samples were analyzed from 24 subjects challenged with either RV-A16 (n = 13) or RV-A39 (n = 11) who became infected, corresponding to three time points (day 0, pre-inoculation; day 4/5, acute infection; and day 21, convalescence).

By first analyzing pooled data for all subjects at all time points using stochastic neighbor embedding (SNE) (van der Maaten and Hinton, 2008), CD19+IgD− cells (total memory B cells and plasmablasts) were classified into five main populations: (1) a major group of

Author Manuscript Author Manuscript Author Manuscript Author Manuscript

CXCR5+ memory B cells; (2) plasmablasts with low CD20 expression; (3) CXCR5− memory B cells with high CD20 expression; (4) a small group expressing CD20 and CD38, suggestive of extrafollicular plasmablasts (PB-X); and (5) contaminating non-B cells with low CD20 expression (Figure 4A). A deeper clustering analysis yielded 50 phenotypes based on differential expression of 35 markers (Van Gassen et al., 2015; Wilkerson and Hayes, 2010) Figure 4B). A heatmap display listed markers in order of priority based on their efficiency to discriminate phenotypes (Figure 4C). Markers were selected that distinguished plasmablasts (CD20 [low], CD22 [low], CD38 [high], CD43 [high], and CD86 [high]) from conventional B cells. Other markers were those expressed on cells that are activated or found at inflamed sites (CD27, CD95, and MHCII) and those involved in cell trafficking (integrins β1 [airway] and β7 [gut], CXCR5 and CCR7 [lymphoid organs], CCR5 and CXCR3 [inflamed airways], and CXCR4 [bone marrow]).

Four memory B cell clusters were identified that lacked expression of CXCR5, which were IgG+ or IgA+, T-bet^{high}, CD11c^{high}, CD19^{high}, and CD20^{high} (designated cluster numbers 19, 20, 25, and 26) (Figure 4C). Dual-specific B cells constituted a single one of these clusters that was IgG+ (cluster 19), and expressed integrin β1, CCR5, and CXCR3, as well as markers of activation/inflammation (CD95^{high}, CD40^{low}, and MHCII^{high}). Inspection of the data revealed that cluster 19 was almost exclusively T-bet+ (92% ± 2%). These cells also expressed low levels of the B cell co-receptor CD21 and high levels of the inhibitory receptor CD22, similar to other reports of T-bet+ tissue-like memory B cells (Knox et al., 2017; Lau et al., 2017; Li et al., 2016; Moir et al., 2008). Virus labeling was not restricted to cluster 19; however, the algorithm assigned all other clusters a log-scaled value for RV signals at least ~80% lower, indicating the presence of much lower numbers of RV-specific B cells (presumably including mono-specific B cells) dispersed across multiple other clusters. Thus, to allow for the assessment of CXCR5+ mono-specific memory B cells, the algorithm was modified for manually gated RV-specific cells only, clustered on the basis of CXCR5 and their labeling with the two virus strains. This analysis confirmed dual-specificity for CXCR5− T-bet+CD11c+ memory B cells and their enrichment for IgG. By contrast, CXCR5+ mono-specific B cells were T-bet^{lo}CD11c^{lo} and CCR7+, consistent with lymph node homing, and CD21 was a prominent feature (Figures 4D and 4E). These findings confirmed the distinctive signature of dual-specific B cells and their tissue homing potential.

Dual-Specific B Cells Expand after RV Infection

Next, we assessed which memory B cell phenotypes were modulated during RV infection by analyzing changes within CD19+IgD− cells. During acute infection (day 4/5 post-inoculation) CXCR5+ circulating memory B cell subsets decreased, consistent with their egress from peripheral blood into lymph nodes (Figure 5A). By contrast, plasmablasts and CXCR5− memory B cell subsets were increased. The largest increase was observed for an extrafollicular plasmablast subset (cluster 38, +50% change over baseline, $p < 0.0001$), consistent with an early extrafollicular response, given its upregulation of CD38 and residual CD20 (hence its designation PB-X) (Figures 4C and 5A–5C) (Fink, 2012). This subset resembled an IgM+ plasmablast, except for its expression of CD20, and displayed low expression of Ki-67, CD27, and CD71, suggesting it had recently differentiated and

Author Manuscript Author Manuscript Author Manuscript Author Manuscript

mobilized but had not undergone mitosis. This subset also expressed β1 integrin and CCR5, indicating the potential to traffic to the airways. The next most significant cluster was an IgA + CXCR5+ memory B cell subset (cluster 41), which decreased by 20% ($p < 0.001$) (Figures 4C and 5A–5C) and whose change was inversely correlated with the increase in cluster 38, indicating a coordinated B cell response ($r = -0.40$, $p < 0.05$) (Figure 5D). Cluster 21 was a similar IgG+ CXCR5+ memory B cell type that also contracted during acute infection (−17%, $p < 0.01$). By contrast, three CXCR5−T-bet+ memory B cell clusters expanded. These included two IgG+ clusters (cluster 20: +15%, $p < 0.01$; and cluster 26: +9%, $p < 0.01$) that differed according to their expression of CD27, CD43, CD95, and CXCR3, as well as an IgA+ cluster (cluster 25: +12%, $p < 0.01$). An IgA+ plasmablast cluster was also expanded at this time point (cluster 1: +16%, $p < 0.01$) (Figures 4C and 5A–5C). The percentage of CD19+IgD− B cells within the B cell compartment was not significantly altered during acute infection.

All clusters that were modulated at day 4 returned to baseline levels by day 21. RV-specific B cells that were dual-specific (cluster 19) constituted the only cluster that significantly increased at day 21 versus day 0 (+23%, $p < 0.001$) (Figures 5A–5C). Further analysis of cluster 19 revealed decreased expression of markers of tissue homing (CXCR3) and inflammation (CD27) during acute infection and their rebound at convalescence, consistent with egress of tissue homing B cells from the periphery, and their subsequent return (Figure S3A). To further examine fluxes in virus-specific B cells that may not be appreciated by the algorithm, mono-specific and dual-specific B cells were analyzed within CXCR5+ and CXCR5− memory subsets by manual gating of mass cytometry data (Figure 5E). As expected, the results confirmed an increase in dual-specific B cells after RV infection, but also revealed increases in mono-specific B cells, when analyzed in relation to challenge with homotypic, but not heterotypic, virus. Similar results were obtained regardless of the RV strain used for challenge (Figure S3B). Together, the findings demonstrated highly coordinated responses of diverse B cell types during RV infection and confirmed the response of dual-specific B cells to heterotypic virus.

Early Antibody Responses to RV in the Nose Are Cross-Reactive, Limited to IgG, and Coincide with Infiltrating Dual-Specific B Cells

To establish a role for B cells at the site of infection, nasal biopsies were obtained during acute infection. Immunohistochemistry analysis revealed dense infiltrates of CD19+CD20+ B cells that co-localized with virus and CD3+ T cells in the nasal mucosa, indicating the presence of memory B cells, rather than plasma cells (Figures 6A, 6B, and S4). B cells were absent in tissue from healthy controls. Flow cytometry analysis confirmed the presence of dual-specific memory B cells (CD20+CD38−) that were predominantly IgG+ (Figures 6C and S5). Nasal B cells also expressed T-bet and CD11c, albeit at lower levels than CXCR5− memory B cells in the blood (Figures 2I–2K, 6C, and S5). This feature, coupled with expression of CD27 and Ki-67, and a downshift in CD20, was consistent with a transition to plasmablasts, similar to B cells cultured under conditions for plasma cell differentiation (Figures 6C, S2, and S5). CXCR5 was not analyzed in nasal B cells owing to the susceptibility of chemokine receptors to enzymatic digestion during the isolation of cells from tissue (Trapecar et al., 2017).

Author Manuscript Author Manuscript Author Manuscript Author Manuscript

Analysis of nasal wash specimens revealed a rapid cross-reactive response that was restricted to IgG, peaked at day 4/5, and was followed by a second peak at day 21 (Figure 6D). These antibodies matched the features of dual-specific B cells. By contrast, increases in strain-specific IgA and IgM were restricted to day 21 and matched the antibody profiles of mono-specific B cells and those in the serum (Figures 1E and 3). Anti-viral responses in the nose were accompanied by weak IgG responses to tetanus, suggesting seepage from serum. Surprisingly, weak anti-viral IgG responses were also detected in the nose of subjects who tested negative for RV infection, suggesting that viral exposure can recruit low numbers of virus-specific memory B cells, without hallmarks of infection (Figure S6). Taken together, these data indicate the rapid recruitment of dual-specific B cells to the nose. The differences in nasal and serum antibody profiles suggest the division of labor between dual-specific and mono-specific B cells in the production of local and systemic antibodies, respectively.

Dual-Specific B Cells Are Clonally Distinct from Their Mono-specific Counterparts

In order to gain further insight into the features of dual-specific B cells and their relationship to mono-specific cells, RV-specific B cell subtypes were purified by cell sorting and subjected to single-cell BCR mRNA sequencing. We theorized that dual-specific B cells would display high rates of hypermutation given their ability to respond to different RV strains and previous reports of increased AICDA transcription in memory B cells sharing their phenotype (Ehrhardt et al., 2008; Knox et al., 2017). As expected, hypermutation was evident for these cells; however, it was highest for IgA+ CXCR5+ cells (Figure 7A). Since IgG1 and IgA1 were the main subclasses expressed by virus-specific B cells, this likely reflects an IgG1 switch to IgA1 (Kitaura et al., 2017), as well as affinity maturation of IgA+ cells in germinal centers.

Given that clonal families of B cells share usage of variable (V), diversity (D), and joining (J) gene segments that encode the BCR, we next compared VDJ segment usage for mono-specific and dual-specific cells. The results revealed a high degree of divergence between antibodies expressed by mono-specific and dual-specific cells, suggesting that dual specificity did not arise from hypermutation of a mono-specific clone, but rather through discrete recombination events in naive B cells (Figure 7B). Moreover, dual-specific cells displayed reduced antibody diversity compared with their mono-specific counterparts. Such oligoclonality of cross-reactive B cells may reflect the evolution of VDJ segments that mediate binding to conserved conformational epitopes of the viral capsid. These findings, coupled with the phenotypic and functional attributes described herein, support the evolution of a discrete cross-reactive tissue homing memory B cell lineage that is rapidly mobilized and expanded in response to different RV strains.

DISCUSSION

Here, we report the first comprehensive analysis of RV-specific B cells and humoral immunity in humans. By using innovative methods that incorporated the use of intact RV capsid to interrogate B cells in parallel with all antibody isotypes, we identified T-bet+ dual-specific cells as candidates for mediating cross-reactive responses to different RV strains in the nose. Our rigorous and multi-faceted approach, applied in both the absence and presence

Author Manuscript Author Manuscript Author Manuscript Author Manuscript

of infection, demonstrated that RV-specific B cells that bound two distinct RV-A strains constituted a major functional subset of CXCR5− memory cells that likely arises from previous RV infections. The pivotal role of dual-specific B cells in the adaptive response was supported by the following observations: (1) their ability to rapidly secrete IgG antibodies specific for both RV-A16 and RV-A39; (2) their outgrowth following *in vivo* infection; (3) their distinctive signature commensurate with preferential migration to tissues; and (4) their enrichment in the nose during infection, concomitant with secreted antibody profiles that define these cells *in vitro.* These collective data indicate that dual-specific T-bet+ B cells are poised to rapidly differentiate and secrete cross-reactive IgG upon infection.

Our findings echo earlier reports of B cell phenotypes capable of exerting effector function in tissues that were referred to as “tissue-like” based on molecular signatures that included the lack of CXCR5 (Ehrhardt et al., 2005; Lau et al., 2017; Li et al., 2016; Moir et al., 2008). A notable characteristic of dual-specific B cells was their expression of the Th1-associated chemokine receptors CCR5 and CXCR3, a feature shared with RV-specific Th1 effector memory cells (Muehling et al., 2016, 2018). Ligands for these receptors are induced by RV in nasal secretions and, thus, would be expected to aid in the coordinated recruitment of dual-specific B cells and Th1 cells to the site of infection (Muehling et al., 2018). In accordance with this, the presence of dual-specific B cells in the nose during acute infection, coupled with the rapid production of cross-reactive IgG antibodies (but not IgA or IgM), supports an effector role for dual-specific B cells in the acute phase. Another notable feature of our system was the dichotomous antibody types and kinetic profiles in the nose versus the serum, which match those antibody profiles of dual-specific and mono-specific B cells, respectively. Together, these findings indicate a spatial and temporal division of labor between distinct virus-specific B cell subsets that mediate antibody responses during the acute phase at the site of infection and those that contribute to the systemic antibody repertoire after virus has cleared.

Despite evidence of their effector function, dual-specific B cells expressed the inhibitory BCR co-receptor CD22. Expression of inhibitory receptors in T-bet+ B cells has been interpreted as a sign of exhaustion (Li et al., 2016; Moir et al., 2008). However, while CD22 inhibits BCR signaling in B cells, it also functions in B cell homeostasis, survival, and migration (Floyd et al., 2000; Nitschke et al., 1997, 1999; Otipoby et al., 1996; Sato et al., 1996). Dual-specific B cells also expressed low levels of the B cell activating molecules CD21 and CD27, similar to tissue-like memory B cells. This phenotype has also been linked to exhaustion based on reduced B cell proliferative capacity, despite the ability to secrete antibodies (Doi et al., 2014). On the other hand, dual-specific B cells also expressed high levels of molecules that amplify BCR signaling (e.g., CD19 and CD20). With these aspects in mind, the functional relevance of inhibitory molecules on dual-specific B cells may be more nuanced in scenarios where alternative pathways (e.g., toll-like receptor) operate to enhance various B cell attributes (Frasca et al., 2017; Jenks et al., 2018; Sohn et al., 2011; Rubtsov et al., 2011). Regardless, when considering our data related to T-bet+ B cells in the RV model in the context of the current literature on similar B cell types, our findings support an effector function for these cells.

Author Manuscript Author Manuscript Author Manuscript Author Manuscript

A novel aspect of our study was the use of intact virus to identify T-bet+ dual-specific B cells. Their recruitment to nasal tissue and subsequent expansion in the blood after *in vivo* infection provided compelling evidence of their relevance to rhinovirus. Additional data to support the specificity of the B cell response is provided by our results related to the capsid subunit VP1 in serum assays, as well as control antigens used in functional assays. Nonetheless, the distinctive signature and binding of different RV strains by dual-specific B cells raises questions regarding their relationship to T-bet+ B cells involved in autoimmune disease (Jenks et al., 2018; Peng et al., 2002; Rubtsova et al., 2017; Wang et al., 2018) that are thought to be "polyreactive." When considering the antigen specificity of such cells, mouse models generally relied on anti-DNA antibodies and tissue damage as a readout of disease; however, the polyreactive nature of antibodies secreted by T-bet+ B cells was not explored. In humans, polyreactive IgG+ B cell clonotypes have been found to secrete antibodies that bind to various antigens including single-stranded DNA, insulin and lipopolysaccharide, and bacteria (Tiller et al., 2007; Wardemann et al., 2003). Recent work identified monoclonal antibodies produced by B cells in the gastrointestinal tract that target the HIV1 envelope, but also cross-react with a number of intestinal proteins. Sequence and/or structural homology was proposed as the molecular basis for this phenomenon (Planchais et al., 2019). We propose that the BCR on the surface of dual-specific B cells recognizes an epitope on the external aspect of the capsid that is shared among different RV strains. Although reactivity with other antigens cannot be definitively excluded, we were unable to demonstrate co-staining of B cells with virus and a variety of unrelated antigens (human and bovine serum albumin, bovine thyroglobulin, murine IgG, and tetanus toxin C-terminal fragment) in preliminary studies. Moreover, B cells failed to bind recombinant RV capsid subunits lacking native conformations. We also tested a wide variety of fluorophores for antigen labeling to minimize background staining and found phycoerythrin to be especially problematic. This is notable given its use to identify polyreactive B cells in early work. Future studies of monoclonal antibodies secreted by RV-specific B cell clonotypes could shed light on the specificity repertoire of these cells.

Our study raises new questions regarding the provenance of dual-specific B cells versus their mono-specific counterparts. One possibility is that these subsets are lineally divergent, a theory supported by their disparate VDJ usage. Indeed, such divergence has been previously appreciated in ABCs and conventional memory (Ellebedy et al., 2016). Furthermore, we identified a rare naive (IgD+) subset that was CXCR5− and T-bet+ that would fit the profile of a precursor dual-specific B cell (data not shown). While the dichotomy of mono- and dual-specificity is puzzling, it is possible that the cross-reactive RV epitope recognized by dual-specific cells, and that drives expansion of these cells at sites of infection, is not maintained on viral antigen priming CXCR5+ B cells that drain to lymph nodes. Variation in the nature of antigen encountered in tissues versus lymph nodes might also explain the different antibody profiles of dual-specific and mono-specific B cells, respectively.

The discrete antibody profiles of mono- and dual-specific B cells were also striking. The interferon axis in the nose would be expected to favor switching of tissue homing dual-specific B cells to IgG. In mice, IFN-γ induces T-bet-dependent class switching to IgG2a in B cells, which is the antibody subclass most closely related to human IgG1 (Mohr et al., 2010; Peng et al., 2002; Rubtsova et al., 2013). On the other hand, we speculate that

Author Manuscript Author Manuscript Author Manuscript Author Manuscript

switching to IgG and IgA in lymph node homing B cells during resolution of RV infection is driven by denatured virus within draining lymph nodes. In addition to its role in antibody switch, T-bet has been implicated in regulating the balance between systemic and mucosal antibody responses, possibly by influencing B cell migration or function via upregulation of CXCR3 (Piovesan et al., 2017; Serre et al., 2012). This might further contribute to the discrepancy between strain-specific antibody profiles in the serum and cross-reactive antibodies in the nose reported here. Interestingly, a similar phenomenon of end-organ tissue cross-reactivity to what we describe has also been found in the lungs of mice infected with influenza (Adachi et al., 2015).

Our collective findings help to explain why humans can resolve RV infections but remain susceptible to re-infection throughout their lives. Adaptive immunity to different RV-A strains is intact in all adults we have tested to date. Beyond B cells, circulating memory T cells that are RV-A specific are cross-reactive, based on their recognition of peptide epitopes that are highly conserved across the RV-A species (Muehling et al., 2016). Repeat infections likely arise from waning of cross-reactive B cell responses overtime, as a result of the return of dual-specific B cells to the circulation, spleen, or other reservoirs. Indeed, our data indicate that nasal B cells are not retained indefinitely, as evidenced by sparse B cells in nasal tissue from healthy controls. Moreover, our data imply that dual-specific B cells fail to give rise to long-lived plasma cells (LLPCs) that might provide durable cross-protection, given that cross-reactive antibody responses in nasal secretions did not extend to the serum. Instead, cross-reactive antibodies are induced locally and briefly, but do not persist systemically, whereas longer-lasting narrow-spectrum antibodies target the infecting strain, but do not cross-protect. This may reflect evolution of the “ideal” relationship between host and virus that is mutually beneficial.

Clinical observations in patients with primary hypogammaglobulinemia provide compelling evidence of the importance of B cells, as opposed to systemic antibodies, in resolving RV infections. This condition results in defects in the production and survival of B cells, and acute respiratory tract infections are common. In these patients, RV was found to be the most common virus, and positive PCR for RV, including that for the same strain, persisted for several months, despite adequate immunoglobulin replacement therapy (Kainulainen et al., 2010). Given that RV-specific antibodies would be expected to be present in the immunoglobulin treatment, owing to high rates of seropositivity to specific RV strains in the population (~40%), this scenario highlights the inability for systemic antibodies to clear virus in the nose, and the importance of antibodies secreted by mucosal B cells.

In addition to study limitations related to the specificity repertoire of dual-specific B cells, questions remain regarding the neutralizing capacity of cross-reactive antibodies in our system. It is possible that conserved epitopes of RV-A16 and RV-A39 are essential for host cell entry via the major RV receptor, ICAM-1. Thus, we might predict that dual-specific B cell clones are more likely to neutralize virus than their mono-specific counterparts. However, neutralization may be dispensable, as long as opsonization occurs. In keeping with the capacity to opsonize virus, we have demonstrated that dual-specific B cells, as well as their secreted antibodies, bind whole virus. It should be noted that the nature of neutralizing antibodies remains ill-defined in RV infection, including their isotype. However, knowledge

Author Manuscript Author Manuscript Author Manuscript Author Manuscript

of antibodies against influenza, another common respiratory viral pathogen, could yield clues. In this context, IgA is more cross-reactive and more neutralizing than IgG, primarily as a result of its more efficient secretion into the airways, and its divalence, which enhances avidity and complex formation with virus (Gould et al., 2017; Muramatsu et al., 2014; Taylor and Dimmock, 1985). Interestingly, whereas IgA outperforms IgG in neutralizing influenza in the upper airways, the reverse may be true in the lower airways during acute infection (Renegar et al., 2004). With respect to RV, neutralizing activity has been detected in nasal secretions as early as 4 days post-infection, consistent with our timeline for the local induction of IgG (Cate et al., 1966).

In summary, we have characterized a novel T-bet+ B cell subset that is cross-reactive for different RV strains. These cells respond rapidly to RV infection *in vivo,* and differ from their mono-specific counterparts based on their tissue homing potential and enrichment for IgG. Through comprehensive assessment of antibody profiles both *in vivo* and *ex vivo* our results implicate dual-specific B cells in the induction of cross-reactive IgG during acute infection, whereas mono-specific B cells drive subsequent IgG, IgA, and IgM responses systemically. Such division of labor among dichotomous B cell types that are virus specific provides unprecedented insight into the B cell response to RV.

STAR★METHODS

Methods that incorporated specified antibodies and reagents are denoted as follows: CyTOF, mass cytometry; FC, flow cytometry; IHC, immunohistochemistry; Multiplex, multiplex serology assay. RRIDs are provided where available.

LEAD CONTACT AND MATERIALS AVAILABILITY

Further information and requests for resources and reagents should be directed to and will be fulfilled by the Lead Contact, Judith Woodfolk (jaw4m@virginia.edu). This study did not generate new unique reagents.

EXPERIMENTAL MODEL AND SUBJECT DETAILS

Human Subjects—Subjects who participated in RV challenge studies were healthy uninfected adults (ages 18–45 years) recruited through the University of Virginia. All subjects were non-allergic based on clinical history or total IgE levels <150 IU/ml, and tested seronegative for the RV challenge strain (serum neutralizing antibody titer ≤ 1:4 for RV-A16 or RV-A39). Numbers, sex and age for each virus were as follows: RV-A16:14 subjects: 4M, 10F, age 21.9 ± 1.9 years; and RV-A39:16 subjects: 4M, 12F, age 21.3 ± 3.7 years. Five of these subjects (1 for RV-A16 and 4 for RV-A39) remained uninfected after RV challenge. Eight additional subjects (5M, 3F, age 22.4 ± 2.3 years) who underwent RV-A16 challenge provided nasal biopsy specimens. Eight healthy uninfected subjects (3M, 5F, age 43.8 ± 18.4 years) not undergoing RV challenge were also recruited through the University of Virginia. Informed consent was obtained from all study participants and subjects were compensated for participation. The research was approved by the Institutional Review Board for Health Sciences Research at the University of Virginia, the Food and Drug Administration, and the National Institute of Allergy and Infectious Diseases Safety

Author Manuscript Author Manuscript Author Manuscript Author Manuscript

Committee. All studies were conducted in compliance with Good Clinical Practices and in accordance with the Declaration of Helsinki.

Experimental Infection Model—Subjects were nasally inoculated with RV-A16 (300$TCID_{50}$) or RV-A39 (100 $TCID_{50}$) (Zambrano et al., 2003; Turner et al., 2017; Agrawal et al., 2014; Muehling et al., 2016, 2018). Blood was drawn for isolation of PBMCs immediately before virus inoculation (baseline, day 0), during the acute infection phase (day 4 or 5), and at convalescence (day 21). Cells were cryopreserved until sample collection was complete. Nasal washes were performed on days 0–5, 7, 14, and 21, and serum was collected at days 0, 4/5, 7 (RV-A16 challenge only), and 21. Nasal biopsy specimens were obtained on day 4 from subjects who received RV-A16 challenge.

Virus Strains—RV-A16 was originally isolated as Strain 11757 from a 2 year old girl in Washington, DC in 1960 (Johnson and Rosen, 1963), and was subsequently numbered as RV16 in 1967 (Kapikian et al., 1967). The RV-A16 challenge pool was derived from an RV-A16 isolate from an infant in Michigan, in 1980 (RV-16, #22478), and a virus challenge pool was produced in 1994 by passage of the original isolate two times in WI-38 cells in the laboratory of Dr. Jack Gwaltney at the University of Virginia. The resulting pool was safety tested according to consensus guidelines for preparation and safety testing of rhinovirus challenge pool (Gwaltney et al., 1992). This pool was subsequently used to infect an 18 year old healthy female volunteer who became the donor of the source virus used for the GMP manufacture of the current RV-A16 challenge pool. Nasal lavage from the donor was transferred to Meridian Life Sciences, Inc., Memphis, TN, where RV-A16 was re-isolated at low passage, safety tested and aliquoted. The resulting pool was submitted to the FDA for review and assigned IND #15162.

RV-A39 was originally isolated as Strain 209 from a patient at the NIH in 1963 (Mufson et al., 1965), and was subsequently numbered as RV39 (Kapikian et al., 1967). The RV-A39 challenge pool was derived from an isolate collected during an epidemiologic study (Gwaltney et al., 1968). The pool was safety tested initially according to then current protocols (Knight, 1964), and subsequently according to updated protocols (Gwaltney et al., 1992). This pool was subsequently used to infect a 20 year old healthy female volunteer who became the donor of the source virus used for the GMP manufacture of the current RV-A39 challenge pool. Nasal lavage from the donor was transferred to Charles River Laboratories, Malvern, PA, where RV-A39 was re-isolated at low passage, safety tested and aliquoted. The resulting pool was submitted to the FDA for review and assigned IND #12934.

METHOD DETAILS

Determination of Infection Status—Neutralizing serum antibodies were evaluated using a standard microtiter assay (Gwaltney et al., 1989), and nasal wash specimens collected on days 1–5 were assessed for the presence of virus using a semiquantitative culture assay or quantitative polymerase chain reaction assay (Turner et al., 1998; Kennedy et al., 2014). Subjects who had at least a 4-fold increase in serum neutralizing antibody to RV-A16 or RV-A39 at day 21, or virus isolated from at least one nasal wash specimen, were considered infected with the study virus (Turner et al., 2017).

Author Manuscript Author Manuscript Author Manuscript Author Manuscript

Preparation of Virus for Assays and Cell Labeling—Cryovials of RV-A16 and RV-A39 were thawed and used to infect HeLa cell monolayers in serum-free minimal essential media, and supplemented with 10% fetal bovine serum after 4 hours (ThermoFisher). After 2 days, virus was released by serial freeze/thawing, cell debris was pelleted and lysates were used for virus purification. Virus was isolated by sucrose cushion (30%), followed by sucrose-gradient (15%−45%), then buffer exchanged into PBS, concentrated, UV-irradiated, and maintained at 4°C (Lee et al., 2015). Capsid integrity was confirmed by electron microscopy, virus purity was assessed by SDS-PAGE analysis with silver staining (Pharmacia PhastSystem), and the virus yield measured by BCA assay (Pierce Chemical Company). RV strain identity was confirmed by RT-PCR specific for the VP1 capsid subunit region of the RNA genome: RV-A16 Forward CATGAATCAGTGTTGGATATTGTGGAC; RV-A16 Reverse AATGTGACCATCTTTGGCTGCTAC; RV-A39 Forward CACTTTCCACAATT ACTATGAAGAAGGAG; RV-A39 Reverse ATCTTCACCTCTTCCAGCTATGCA.

Concentrated virus was diluted to 0.5 μg/μL in 200 μL stock volumes and cryopreserved prior to use. For the purposes of detecting RV-specific B cells in cytometric experiments, virus was tagged at lysine residue terminal amines with Alexa Fluor 488 NHS Ester and Alexa Fluor 568 NHS Ester (ThermoFisher) for multi-color flow cytometry, or else tagged with isotopically enriched cisplatin 194 and 198 (Fluidigm) for mass cytometry (Mei et al., 2016). For serology assays, virus was biotinylated with NHS-LC-Biotin (ThermoFisher). Excess label was desalted on Zeba spin columns to exclude molecular weights below 40kD (ThermoFisher).

Multiplex Serology Assay—Streptavidin-coated polystyrene beads (Spherotech) were first labeled with Alexa Fluor 405 (ThermoFisher) and/or Fixable Viability Stain 510 (BD Biosciences) to create four different fluorescent signatures. Beads were then coated with biotinylated virus (RV-A16 or RV-A39), tetanus toxin c-terminal fragment (positive control), or mouse IgG (negative control), respectively. Beads were then washed and combined, and incubated with serum diluted 250x, nasal washes diluted 10x, or culture supernatants diluted 10x. After washing, antibody binding was detected using anti-human IgG (BD Biosciences), IgM (BioLegend), IgA (Miltenyi), and IgE (BD Biosciences) isotypes. Beads were read on an Invitrogen Attune cytometer.

Multi-color Flow Cytometry—For analysis of B cells from blood, cultures or nasal tissue, cell samples were simultaneously Fc-blocked with unlabeled mouse IgG (Lampire) and ICAM-1-blocked with anti-ICAM-1, (BioLegend), which was fluorescently-labeled or not, depending upon the experiment. After 30 minutes at 4°C, B cells were stained with fluorescently tagged virus (Alexa Fluor 488-RV-A39 and Alexa Fluor 568-RV-A16), viability dye Live/Dead Aqua (ThermoFisher), and various combinations of the following fluorescent antibodies depending on the sample type and application: anti-CD3 (BioLegend), anti-CD11c (BioLegend), anti-CD19 (BioLegend), anti-CD20 (BioLegend), anti-CD27 (ThermoFisher), anti-CD38 (Becton Dickinson), anti-CCR5 (ThermoFisher), anti-CXCR3 (BioLegend), anti-CXCR5 (BioLegend), anti-IgD (ThermoFisher), anti-IgM (BioLegend), anti-IgG (BD Biosciences), anti-IgA (Miltenyi), and anti-IgE (BioLegend).

Author Manuscript Author Manuscript Author Manuscript Author Manuscript

After incubating for 30 minutes at 4°C, cells were then fixed and permeabilized (FoxP3 fix/perm kit, ThermoFisher), before staining for intracellular IgM (BioLegend), IgG (Becton Dickinson), IgA (Miltenyi), IgE (BioLegend), Ki-67 (BioLegend), and T-bet (BioLegend). Cells were analyzed on an LSR Fortessa Cytometer (Becton Dickinson) using FlowJo version 10.5.3 (TreeStar). (See Table S1).

Mass Cytometry—For analysis of circulating B cells during experimental infection, PBMCs were thawed in CTL buffer (Immunospot) with benzonase (Millipore), and acid-stripped of Fc-receptor-bound immunoglobulin. Cells were then barcoded using a 70-fold panel according to an 8 choose 4 scheme (Figure S7) with combined anti-CD45 and anti-MHCI antibodies (BioLegend) bearing 102Pd, 104Pd, 105Pd, 106Pd, 108Pd, 110Pd, 190Os, and/or 192Os (BuyIsotope) (Hartmann et al., 2018; Mei et al., 2015; Zunder et al., 2015). Simultaneously with barcoding, cells were stained with magnetic bead-conjugated antibodies against CD3, CD14, CD16, CD123, and CD235a (Miltenyi), labeled for viability using a 103Rh DNA intercalator (Fluidigm), Fc-blocked with mouse IgG (Lampire), and ICAM-1-blocked (BioLegend). After incubation for 30 minutes at 4° C, samples were combined and sorted for the negative fraction on an autoMACSpro (Miltenyi). Magnetically enriched B cells (30 to 50% CD19+) were then stained for surface proteins using metal-tagged antibodies, and incubated with cisplatin-labeled virus. After 30 minutes at 4°C, staining for intracellular markers was carried out using FoxP3 fix/perm kit (eBioscience). The complete panel for mass cytometry comprised an additional 45 markers, beyond barcoding and viability (see Table S2). Antibodies not purchased pre-conjugated through Fluidigm were tagged with metal isotopes using Fluidigm conjugation kits. Multiplexed samples were read on a CyTOF2 (Fluidigm) and deconvoluted (computationally separated) prior to analysis. Fluctuations in B cell populations were monitored overtime in an unbiased manner using t-SNE dimensionality reduction analysis (van der Maaten and Hinton, 2008) and a clustering workflow (Nowicka et al., 2017) combining FlowSOM self-organizing maps and ConsensusClusterPlus (Van Gassen et al., 2015; Wilkerson and Hayes, 2010; Weber and Robinson, 2016). By this method, similarity to 100 phenotype vectors was scored to generate map coordinates, and cells were clustered into nodes on the basis of density across the map.

Plasmablast Differentiation Culture—Freshly isolated PBMCs were labeled for flow cytometry as described for circulating RV-specific B cells, but were additionally labeled with magnetic bead-conjugated antibodies against CD3, CD14, CD16, CD123, and CD235a (Miltenyi) during the initial blocking step. Samples were then enriched for B cells by negative fractionation on an autoMACSpro (Miltenyi). Enriched B cells (30 to 50% CD19+) were then stained using an abbreviated panel of CD3, CD19, CD20, IgD, CXCR5, RV-A16, and RV-A39, omitting fix/perm steps. RV-16-specific, RV-39-specific, dual-specific, non-specific naive (IgD+), non-specific CXCR5+ memory (IgD-), and non-specific CXCR5− memory (IgD-) B cells (CD19+ CD20+ CD3-) were purified on an Influx Cell Sorter (Becton Dickinson) to > 90% purity (Figure S6). Following isolation, 3–5,000 cells (RV-specific subsets) or 10,000 cells (other B cell subsets) were plated and cultured for 10 days in IMDM supplemented with 10% FBS, non-essential amino acids, insulin/transferrin/selenium, β-mercaptoethanol, 500 ng/ml anti-CD40 (BioLegend), 600 IU/ml IL-2

Author Manuscript Author Manuscript Author Manuscript Author Manuscript

(Miltenyi), 25ng/ml IL-10 (Miltenyi), 100ng/ml IL-21 (Miltenyi), and 2.5 μg/ml ODN 2006 (Miltenyi) (Karahan et al., 2014). Supernatants were collected every two days, and tested for secreted antibodies by bead-based multiplex assay. An aliquot of cells was harvested every 2 days for analysis by flow cytometry.

Fluorescence Microscopy—Nasal biopsies were obtained from infected subjects at 4 days post-challenge with RV-A16. Biopsies were obtained from the inferior turbinate, the middle turbinate, and the posterior nasopharynx. Leftover tissue from nasal biopsies obtained from uninfected subjects as part of their routine clinical care was used as a control. All tissue was fixed in formalin, paraffin embedded, and sectioned. Prior to staining, sections were deparaffinized in xylene, washed in 100% ethanol, and gradually transitioned to water. Epitope retrieval was conducted in citrate pH6 buffer (Abcam) at 100.5°C for 20 minutes. Slides were then blocked with 10% donkey serum (Southern Biotech), labeled with primary antibodies against CD3 (rabbit, ThermoFisher), CD11c (rabbit, Abcam), CD19 (rat, ThermoFisher), CD20 (mouse, BioPrime), RV-A16 VP2 (mouse, QED Bioscience), and/or T-bet (mouse, BioLegend) (or mouse, rat, and rabbit isotype controls from ThermoFisher) at 5ug/mL, reblocked, and stained with 5ug/mL donkey anti-mouse, donkey anti-rat, or donkey anti-rabbit antibodies (ThermoFisher Scientific) tagged with Alexa Fluor 488 NHS Ester (ThermoFisher), tetramethylrhodamine NHS Ester (ThermoFisher), or Alexa Fluor 647 NHS Ester (ThermoFisher) respectively. Specimens were counterstained with DAPI at 1ug/mL (PromoKine)(see also Table S1). Imaging was performed on a Zeiss Axioimager with Apotome attachment using Zeiss optical filter numbers 49 (DAPI), 38HE (Alexa Fluor 488), 43HE (tetramethylrhodamine), and 50 (Alexa Fluor 647).

Isolation of B Cells from Nasal Biopsies—Fresh nasal biopsies were obtained from the inferior turbinates of infected subjects at 4 days post-challenge with RV-A16. Tissue was incubated with agitation for 1 hour at 37°C in RPMI 1640 media +2% FBS, supplemented with 80mg/L (0.4kU/L) Liberase TM (Collagenase I+II, SigmaAldrich), and 100mg/L (270kU/L) DNase I (SigmaAldrich). PBMCs from a single donor were subjected to the same treatment as a control. Cells were isolated by pipetting digested samples through 40μm filters, and then analyzed by flow cytometry.

Single-Cell mRNA Sequencing—Circulating RV-specific B cells (CD19+CD20+) isolated from a healthy uninfected subject (male, 33 years) were identified by multi-color flow cytometry, and sorted on an Influx Cell Sorter (Beckton Dickinson) based on differential expression of CXCR5, and whether or not they were mono- or dual-specific. Sorted cells were immediately processed for single-cell V(D)J mRNA profiling by barcoding on a Chromium Controller, amplifying pooled cDNA and targeting enrichment for full-length V(D)J segments using primers specific to Ig constant regions (10xGenomics). Yields were quantified on a Qubit fluorometer (Invitrogen), quality assessed by Tape Station (Agilent), and amplified by PCR. Next-generation sequencing was performed by MiSeq (Illumina). Reads were mapped to a human reference using Cellranger software (10xGenomics) and analyzed for somatic hypermutation and VDJ segment usage on vLoupe browser (10xGenomics). Mutations were compared for RV-specific subsets that were categorized based on antibody isotypes expressed.

Author Manuscript Author Manuscript Author Manuscript Author Manuscript

QUANTIFICATION AND STATISTICAL ANALYSIS

Change in serum antibodies and the percentage/MFI of different B cell subsets during the course of RV infection were analyzed using the Wilcoxon matched pairs signed-rank test. Change in antibody levels in B cell culture supernatants were analyzed by the Friedman multiple comparisons test. Mann-Whitney ranked-sum test was used to analyze cell counts in nasal biopsies from different subjects and mutations in different immunoglobulin isotypes. Spearman correlation was used to test the relationship between the change in percentages for discrete B cell subsets during infection. Significant changes in B cell clusters detected by mass cytometry were designated at a level of $p < 0.01$ for stringency. A p value < 0.05 was considered significant for all other parameters tested. Statistical analysis was conducted using GraphPad Prism software (Graph Pad Software Inc. CA). Statistical details for each experiment are located in the results, figures, and figure legends.

DATA AND CODE AVAILABILITY

The accession number for the RNA-sequencing data reported in this paper is PRJNA580187 at the NIH NCBI Sequence Read Archive.

ADDITIONAL RESOURCES

RV challenges were performed under clinical trials with the following registry ID numbers: NCT02111772; NCT01669603 and NCT02910401 located at https://clinicaltrials.gov/.

Supplementary Material

Refer to Web version on PubMed Central for supplementary material.

ACKNOWLEDGMENTS

This work was funded by NIH/NIAID grants U01 AI100799, U01 AI125056, U01 AI123337, R01 AI020565, R21 AI138077, and T32 AI007496; and by Danisco Sweeteners Oy, Kantvik, Finland (part of Dupont Nutrition & Biosciences). The authors would like to thank Joanne Lannigan, MS, Claude Chew, BS, and Michael Solga, MS (University of Virginia Flow Cytometry Core Facility), for their help with mass cytometry and cell sorting; Katia Sol-Church, PhD (University of Virginia Genome Analysis and Technology Core), for assistance with single-cell Mrna sequencing; Eli Zunder, PhD, for contributing Pd isotopes for initial barcoding testing; Jennifer Ju, MD, and Robin Legallo, MD, for assisting with histology; Theo Rispens, PhD, for his generous contribution of anti-human mIgG4 antibody; Rudolph Valenta, MD, and Katarzyna Niespodziana, PhD, for their generous contribution of recombinant RV-A16 capsid subunit proteins; Judith White, PhD, and Elizabeth Nelson, MS, for sharing expertise in virus purification; Elizabeth Opila, PhD, and Lucas Herweyer, BA, for help measuring osmium chloride concentrations by ICP-OES; Joel Herbein, PhD, for the generous contribution of tetanus toxin c-terminal fragment; and Cheree Denby, Deborah Murphy, RN, Holliday Carper, BS, and Marcia Ripley, BS, for assisting with study coordination.

REFERENCES

Adachi Y, Onodera T, Yamada Y, Daio R, Tsuiji M, Inoue T, Kobayashi K, Kurosaki T, Ato M, and Takahashi Y (2015). Distinct germinal center selection at local sites shapes memory B cell response to viral escape. J. Exp. Med 212, 1709–1723. [PubMed: 26324444]

Agrawal R, Wisniewski J, Yu MD, Kennedy JL, Platts-Mills T, Heymann PW, and Woodfolk JA (2014). Infection with human rhinovirus 16 promotes enhanced IgE responsiveness in basophils of atopic asthmatics. Clin. Exp. Allergy 44, 1266–1273. [PubMed: 25113532]

Barclay WS, al-Nakib W, Higgins PG, and Tyrrell DA (1989). The time course of the humoral immune response to rhinovirus infection. Epidemiol. Infect 103, 659–669. [PubMed: 2558033]

Author Manuscript Author Manuscript Author Manuscript Author Manuscript

Barnett BE, Staupe RP, Odorizzi PM, Palko O, Tomov VT, Mahan AE, Gunn B, Chen D, Paley MA, Alter G, et al. (2016). Cutting Edge: B cell-intrinsic T-bet expression Is required to control chronic viral infection. J. Immunol 197, 1017–1022. [PubMed: 27430722]

Bertino JS (2002). Cost burden of viral respiratory infections: issues for formulary decision makers. Am. J. Med 112 (Suppl 6A), 42S–49S. [PubMed: 11955459]

Breitfeld D, Ohl L, Kremmer E, Ellwart J, Sallusto F, Lipp M, and Förster R (2000). Follicular B helper T cells express CXC chemokine receptor 5, localize to B cell follicles, and support immunoglobulin production. J. Exp. Med 192, 1545–1552. [PubMed: 11104797]

Calhoun WJ, Dick EC, Schwartz LB, and Busse WW (1994). A common cold virus, rhinovirus 16, potentiates airway inflammation after segmental antigen bronchoprovocation in allergic subjects. J. Clin. Invest 94, 2200–2208. [PubMed: 7989575]

Cate TR, Rossen RD, Douglas RG Jr., Butler WT, and Couch RB (1966). The role of nasal secretion and serum antibody in the rhinovirus common cold. Am. J. Epidemiol 84, 352–363. [PubMed: 4288191]

Chang L-Y, Li Y, and Kaplan DE (2017). Hepatitis C viraemia reversibly maintains subset of antigen-specific T-bet+ tissue-like memory B cells. J. Viral Hepat 24, 389–396. [PubMed: 27925349]

Ding Y, Rui B, Gao C, Xu M, Wang L, Zhao C, Bai J, Wang J, Xu J, and Pan W (2018). Non-neutralizing antibody responses against VP1 in enterovirus A, B, C and rhinovirus A species among infants and children in Shanghai. Sci. Rep 8, 5455. [PubMed: 29615683]

Doi H, Tanoue S, and Kaplan DE (2014). Peripheral CD27-CD21- B-cells represent an exhausted lymphocyte population in hepatitis C cirrhosis. Clin. Immunol 150, 184–191. [PubMed: 24434272]

Doria-Rose NA, Klein RM, Manion MM, O'Dell S, Phogat A, Chakrabarti B, Hallahan CW, Migueles SA, Wrammert J, Ahmed R, et al. (2009). Frequency and phenotype of human immunodeficiency virus envelope-specific B cells from patients with broadly cross-neutralizing antibodies. J. Virol 83, 188–199. [PubMed: 18922865]

Dullaers M, Li D, Xue Y, Ni L, Gayet I, Morita R, Ueno H, Palucka KA, Banchereau J, and Oh S (2009). A T cell-dependent mechanism for the induction of human mucosal homing immunoglobulin A-secreting plasmablasts. Immunity 30, 120–129. [PubMed: 19144318]

Ehrhardt GRA, Hsu JT, Gartland L, Leu C-M, Zhang S, Davis RS, and Cooper MD (2005). Expression of the immunoregulatory molecule FcRH4 defines a distinctive tissue-based population of memory B cells. J. Exp. Med 202, 783–791. [PubMed: 16157685]

Ehrhardt GRA, Hijikata A, Kitamura H, Ohara O, Wang J-Y, and Cooper MD (2008). Discriminating gene expression profiles of memory B cell subpopulations. J. Exp. Med 205, 1807–1817. [PubMed: 18625746]

Ellebedy AH, Jackson KJL, Kissick HT, Nakaya HI, Davis CW, Roskin KM, McElroy AK, Oshansky CM, Elbein R, Thomas S, et al. (2016). Defining antigen-specific plasmablast and memory B cell subsets in human blood after viral infection or vaccination. Nat. Immunol 17, 1226–1234. [PubMed: 27525369]

Fendrick AM, Monto AS, Nightengale B, and Sarnes M (2003). The economic burden of non-influenza-related viral respiratory tract infection in the United States. Arch. Intern. Med 163, 487–494. [PubMed: 12588210]

Fink F (2012). Origin and function of circulating plasmablasts during acute viral infections. Front. Immunol 3, 78. [PubMed: 22566959]

Fleet WF, Couch RB, Cate TR, and Knight V (1965). Homologous and heterologous resistance to rhinovirus common cold. Am. J. Epidemiol 82, 185–196. [PubMed: 4283952]

Floyd H, Nitschke L, and Crocker PR (2000). A novel subset of murine B cells that expresses unmasked forms of CD22 is enriched in the bone marrow: implications for B-cell homing to the bone marrow. Immunology 101, 342–347. [PubMed: 11106937]

Franz B, May KF Jr., Dranoff G, and Wucherpfennig K (2011). Ex vivo characterization and isolation of rare memory B cells with antigen tetramers. Blood 118, 348–357. [PubMed: 21551230]

Frasca D, Diaz A, Romero M, D'Eramo F, and Blomberg BB (2017). Aging effects on T-bet expression in human B cell subsets. Cell. Immunol 321, 68–73. [PubMed: 28457482]

Author Manuscript Author Manuscript Author Manuscript Author Manuscript

Glanville N, and Johnston SL (2015). Challenges in developing a cross-serotype rhinovirus vaccine. Curr. Opin. Virol 11, 83–88. [PubMed: 25829255]

Gould VMW, Francis JN, Anderson KJ, Georges B, Cope AV, and Tregoning JS (2017). Nasal IgA provides protection against human influenza challenge in volunteers with low serum influenza antibody titre. Front. Microbiol 8, 900. [PubMed: 28567036]

Gwaltney JM Jr., Hendley JO, Simon G, and Jordan WS Jr. (1968). Rhinovirus infections in an industrial population. 3. Number and prevalence of serotypes. Am. J. Epidemiol. 87, 158–166. [PubMed: 4295427]

Gwaltney J, Colonno R, Hamparian V, and Turner R (1989). Rhinovirus. In Diagnostic Procedures for Viral, Rickettsial, and Chlamydial Infections, Schmidt N and Emmons R, eds. (American Public Health Association), pp.579–614.

Gwaltney JM Jr., Hendley O, Hayden FG, McIntosh K, Hollinger FB, Melnick JL, and Turner RB (1992). Updated recommendations for safety-testing of viral inocula used in volunteer experiments on rhinovirus colds. Prog. Med. Virol 39, 256–263. [PubMed: 1317600]

Hao Y, O'Neill P, Naradikian MS, Scholz JL, and Cancro MP (2011). A B-cell subset uniquely responsive to innate stimuli accumulates in aged mice. Blood 118, 1294–1304. [PubMed: 21562046]

Hargreaves DC, Hyman PL, Lu TT, Ngo VN, Bidgol A, Suzuki G, Zou YR, Littman DR, and Cyster JG (2001). A coordinated change in chemokine responsiveness guides plasma cell movements. J. Exp. Med 194, 45–56. [PubMed: 11435471]

Hartmann FJ, Simonds EF, and Bendall SC (2018). A universal live cell barcoding-platform for multiplexed human single cell analysis. Sci. Rep 8, 10770. [PubMed: 30018331]

Hendley JO (1998). Epidemiology, pathogenesis, and treatment of the common cold. Semin. Pediatr. Infect. Dis 9, 50–55.

Iwane MK, Prill MM, Lu X, Miller EK, Edwards KM, Hall CB, Griffin MR, Staat MA, Anderson LJ, Williams JV, et al. (2011). Human rhinovirus species associated with hospitalizations for acute respiratory illness in young US children. J. Infect. Dis 204, 1702–1710. [PubMed: 22013207]

Iwasaki J, Smith WA, Khoo SK, Bizzintino J, Zhang G, Cox DW, Laing IA, Le Souëf PN, Thomas WR, and Hales BJ (2014). Comparison of rhinovirus antibody titers in children with asthma exacerbations and species-specific rhinovirus infection. J. Allergy Clin. Immunol 134, 25–32. [PubMed: 24767874]

Jacobs SE, Lamson DM, St George K, and Walsh TJ (2013). Human rhinoviruses. Clin. Microbiol. Rev 26, 135–162. [PubMed: 23297263]

Jenks SA, Cashman KS, Zumaquero E, Marigorta UM, Patel AV, Wang X, Tomar D, Woodruff MC, Simon Z, Bugrovsky R, et al. (2018). Distinct effector B cells induced by unregulated toll-like Receptor 7 contribute to pathogenic responses in systemic lupus erythematosus. Immunity 49, 725–739.e6. [PubMed: 30314758]

Johnson KM, and Rosen L (1963). Characteristics of five newly recognized enteroviruses recovered from the human oropharynx. Am. J. Hyg 77, 15–25.

Kainulainen L, Vuorinen T, Rantakokko-Jalava K, Österback R, and Ruuskanen O (2010). Recurrent and persistent respiratory tract viral infections in patients with primary hypogammaglobulinemia. J. Allergy Clin. Immunol 126, 120–126. [PubMed: 20541246]

Kallies A, and Good-Jacobson KL (2017). Transcription Factor T-bet Orchestrates Lineage Development and Function in the Immune System. Trends Immunol. 38, 287–297. [PubMed: 28279590]

Kapikian AZ, Conant RM, Hamparian VV, Chanock RM, Chapple PJ, Dick EC, Fenters JD, Gwaltney JM Jr., Hamre D, Holper JC, et al. (1967). Rhinoviruses: a numbering system. Nature 213, 761–762. [PubMed: 4291698]

Karahan GE, Eikmans M, Anholts JDH, Claas FHJ, and Heidt S (2014). Polyclonal B cell activation for accurate analysis of pre-existing antigen-specific memory B cells. Clin. Exp. Immunol 177, 333–340. [PubMed: 24611883]

Karnell JL, Kumar V, Wang J, Wang S, Voynova E, and Ettinger R (2017). Role of $CD11c^{+}$ $T\text{-}bet^{+}$B cells in human health and disease. Cell. Immunol 321, 40–45. [PubMed: 28756897]

Author Manuscript Author Manuscript Author Manuscript Author Manuscript

Kennedy JL, Shaker M, McMeen V, Gern J, Carper H, Murphy D, Lee WM, Bochkov YA, Vrtis RF, Platts-Mills T, et al. (2014). Comparison of viral load in individuals with and without asthma during infections with rhinovirus. Am. J. Respir. Crit. Care Med 189, 532–539. [PubMed: 24471509]

Kitaura K, Yamashita H, Ayabe H, Shini T, Matsutani T, and Suzuki R (2017). Different somatic hypermutation levels among antibody subclasses disclosed by a new next-generation sequencing-based antibody repertoire analysis. Front. Immunol. 8, 389. [PubMed: 28515723]

Knight V (1964). The Use of Volunteers in Medical Virology In Medical Virology, Melnick JL, ed. (Karger), pp. 1–26.

Knox JJ, Buggert M, Kardava L, Seaton KE, Eller MA, Canaday DH, Robb ML, Ostrowski MA, Deeks SG, Slifka MK, et al. (2017). T-bet^{+} B cells are induced by human viral infections and dominate the HIV gp140 response. JCI Insight 2, 8.

Lanzavecchia A, Parodi B, and Celada F (1983).Activation of human B lymphocytes: frequency of antigen-specific B cells triggered by alloreactive or by antigen-specific T cell clones. Eur. J. Immunol 13, 733–738. [PubMed: 6604634]

Lau D, Lan LY-L, Andrews SF, Henry C, Rojas KT, Neu KE, Huang M, Huang Y, DeKosky B, Palm A-KE, et al. (2017). Low CD21 expression defines a population of recent germinal center graduates primed for plasma cell differentiation. Sci. Immunol 2, eaai8153. [PubMed: 28783670]

Lazarevic V, Glimcher LH, and Lord GM (2013). T-bet: a bridge between innate and adaptive immunity. Nat. Rev. Immunol 13, 777–789. [PubMed: 24113868]

Lebrun A, Portocarrero C, Kean RB, Barkhouse DA, Faber M, and Hooper DC (2015). T-bet is required for the rapid clearance of attenuated rabies virus from central nervous system tissue. J. Immunol 195, 4358–4368. [PubMed: 26408670]

Lee W-M, Chen Y, Wang W, and Mosser A (2015). Growth of human rhinovirus in H1-HeLa cell suspension culture and purification of virions. Methods Mol. Biol 1221, 49–61. [PubMed: 25261306]

Li H, Borrego F, Nagata S, and Tolnay M (2016). Fc receptor-like 5 expression distinguishes two distinct subsets of human circulating tissue-like memory B cells. J. Immunol. 196, 4064–4074. [PubMed: 27076679]

Manni M, Gupta S, Ricker E, Chinenov Y, Park SH, Shi M, Pannellini T, Jessberger R, Ivashkiv LB, and Pernis AB (2018). Regulation of age-associated B cells by IRF5 in systemic autoimmunity. Nat. Immunol 19, 407–419. [PubMed: 29483597]

Megremis S, Niespodziana K, Cabauatan C, Xepapadaki P, Kowalski ML, Jartti T, Bachert C, Finotto S, West P, Stamataki S, et al. (2018). Rhinovirus species-specific antibodies differentially reflect clinical outcomes in health and asthma. Am. J. Respir. Crit. Care Med 198, 1490–1499.

Mei HE, Leipold MD, Schulz AR, Chester C, and Maecker HT (2015). Barcoding of live human peripheral blood mononuclear cells for multiplexed mass cytometry. J. Immunol 194, 2022–2031. [PubMed: 25609839]

Mei HE, Leipold MD, and Maecker HT (2016). Platinum-conjugated antibodies for application in mass cytometry. Cytometry A 89, 292–300. [PubMed: 26355391]

Mohr E, Cunningham AF, Toellner K-M, Bobat S, Coughlan RE, Bird RA, MacLennan ICM, and Serre K (2010). IFN-γ produced by CD8 T cells induces T-bet-dependent and -independent class switching in B cells in responses to alum-precipitated protein vaccine. Proc. Natl. Acad. Sci. USA 107, 17292–17297. [PubMed: 20855629]

Moir S, Ho J, Malaspina A, Wang W, DiPoto AC, O'Shea MA, Roby G, Kottilil S, Arthos J, Proschan MA, et al. (2008). Evidence for HIV-associated B cell exhaustion in a dysfunctional memory B cell compartment in HIV-infected viremic individuals. J. Exp. Med 205, 1797–1805. [PubMed: 18625747]

Muehling LM, Mai DT, Kwok WW, Heymann PW, Pomés A, and Woodfolk JA (2016). Circulating Memory CD4+ T Cells Target Conserved Epitopes of Rhinovirus Capsid Proteins and Respond Rapidly to Experimental Infection in Humans. J. Immunol 197, 3214–3224. [PubMed: 27591323]

Muehling LM, Turner RB, Brown KB, Wright PW, Patrie JT, Lahtinen SJ, Lehtinen MJ, Kwok WW, and Woodfolk JA (2018). Single-cell tracking reveals a role for pre-existing CCR5+ memory Th1

Author Manuscript Author Manuscript Author Manuscript Author Manuscript

cells in the control of rhinovirus-A39 after experimental challenge in humans. J. Infect. Dis 217, 381–392. [PubMed: 29309618]

Mufson MA, Kawana R, James HD Jr., Gauld LW, Bloom HH, and Chanock RM (1965). A description of six new rhinoviruses of human origin. Am. J. Epidemiol 81, 32–43. [PubMed: 14246079]

Muramatsu M, Yoshida R, Yokoyama A, Miyamoto H, Kajihara M, Maruyama J, Nao N, Manzoor R, and Takada A (2014). Comparison of antiviral activity between IgA and IgG specific to influenza virus hemagglutinin: increased potential of IgA for heterosubtypic immunity. PLoS ONE 9, e85582. [PubMed: 24465606]

Nichol KL, D'Heilly S, and Ehlinger E (2005). Colds and influenza-like illnesses in university students: impact on health, academic and work performance, and health care use. Clin. Infect. Dis 40, 1263–1270. [PubMed: 15825028]

Niespodziana K, Napora K, Cabauatan C, Focke-Tejkl M, Keller W, Niederberger V, Tsolia M, Christodoulou I, Papadopoulos NG, and Valenta R (2012). Misdirected antibody responses against an N-terminal epitope on human rhinovirus VP1 as explanation for recurrent RV infections. FASEB J. 26, 1001–1008. [PubMed: 22121050]

Nitschke L, Carsetti R, Ocker B, Köhler G, and Lamers MC (1997). CD22 is a negative regulator of B-cell receptor signalling. Curr. Biol 7, 133–143. [PubMed: 9016707]

Nitschke L, Floyd H, Ferguson DJ, and Crocker PR (1999). Identification of CD22 ligands on bone marrow sinusoidal endothelium implicated in CD22-dependent homing of recirculating B cells. J. Exp. Med 189, 1513–1518. [PubMed: 10224292]

Nowicka M, Krieg C, Crowell HL, Weber LM, Hartmann FJ, Guglietta S, Becher B, Levesque MP, and Robinson MD (2017). CyTOF workflow: differential discovery in high-throughput high-dimensional cytometry datasets. F1000Res. 6, 748. [PubMed: 28663787]

Okada T, Ngo VN, Ekland EH, Förster R, Lipp M, Littman DR, and Cyster JG (2002). Chemokine requirements for B cell entry to lymph nodes and Peyer's patches. J. Exp. Med 196, 65–75. [PubMed: 12093871]

Otipoby KL, Andersson KB, Draves KE, Klaus SJ, Farr AG, Kerner JD, Perlmutter RM, Law CL, and Clark EA (1996). CD22 regulates thymus-independent responses and the lifespan of B cells. Nature 384, 634–637. [PubMed: 8967951]

Peng SL, Szabo SJ, and Glimcher LH (2002). T-bet regulates IgG class switching and pathogenic autoantibody production. Proc. Natl. Acad. Sci. USA 99, 5545–5550. [PubMed: 11960012]

Piovesan D, Tempany J, Di Pietro A, Baas I, Yiannis C, O'Donnell K, Chen Y, Peperzak V, Belz GT, Mackay CR, et al. (2017). c-Myb Regulates the T-Bet-Dependent Differentiation Program in B Cells to Coordinate Antibody Responses. Cell Rep. 19, 461–470. [PubMed: 28423310]

Planchais C, Kök A, Kanyavuz A, Lorin V, Bruel T, Guivel-Benhassine F, Rollenske T, Prigent J, Hieu T, Prazuck T, et al. (2019). HIV-1 Envelope Recognition by Polyreactive and Cross-Reactive Intestinal B Cell. Cell Rep. 27, 572–585.e7. [PubMed: 30970259]

Portugal S, Tipton CM, Sohn H, Kone Y, Wang J, Li S, Skinner J, Virtaneva K, Sturdevant DE, Porcella SF, et al. (2015). Malaria-associated atypical memory B cells exhibit markedly reduced B cell receptor signaling and effector function. eLife 4, e07218.

Renegar KB, Small PA Jr., Boykins LG, and Wright PF (2004). Role of IgA versus IgG in the control of influenza viral infection in the murine respiratory tract. J. Immunol 173, 1978–1986. [PubMed: 15265932]

Roelen CAM, Koopmans PC, Notenbomer A, and Groothoff JW (2011). Job satisfaction and short sickness absence due to the common cold. Work 39, 305–313. [PubMed: 21709366]

Rubtsov AV, Rubtsova K, Fischer A, Meehan RT, Gillis JZ, Kappler JW, and Marrack P (2011). Toll-like receptor 7 (TLR7)-driven accumulation of a novel CD11c^{+} B-cell population is important for the development of autoimmunity. Blood 118, 1305–1315. [PubMed: 21543762]

Rubtsova K, Rubtsov AV, van Dyk LF, Kappler JW, and Marrack P (2013). T-box transcription factor T-bet, a key player in a unique type of B-cell activation essential for effective viral clearance. Proc. Natl. Acad. Sci. USA 110, E3216–E3224. [PubMed: 23922396]

Rubtsova K, Rubtsov AV, Thurman JM, Mennona JM, Kappler JW, and Marrack P (2017). B cells expressing the transcription factor T-bet drive lupus-like autoimmunity. J. Clin. Invest 127, 1392–1404. [PubMed: 28240602]

Author Manuscript Author Manuscript Author Manuscript Author Manuscript

Sato S, Miller AS, Inaoki M, Bock CB, Jansen PJ, Tang ML, and Tedder TF (1996). CD22 is both a positive and negative regulator of B lymphocyte antigen receptor signal transduction: altered signaling in CD22-deficient mice. Immunity 5, 551–562. [PubMed: 8986715]

Serre K, Cunningham AF, Coughlan RE, Lino AC, Rot A, Hub E, Moser K, Manz R, Ferraro A, Bird R, et al. (2012). CD8 T cells induce T-bet-dependent migration toward CXCR3 ligands by differentiated B cells produced during responses to alum-protein vaccines. Blood 120, 4552–4559. [PubMed: 23065152]

Sohn HW, Krueger PD, Davis RS, and Pierce SK (2011). FcRL4 acts as an adaptive to innate molecular switch dampening BCR signaling and enhancing TLR signaling. Blood 118, 6332–6341. [PubMed: 21908428]

Taylor HP, and Dimmock NJ (1985). Mechanism of neutralization of influenza virus by secretory IgA is different from that of monomeric IgA or IgG. J. Exp. Med 161, 198–209. [PubMed: 2981953]

Tiller T, Tsuiji M, Yurasov S, Velinzon K, Nussenzweig MC, and Wardemann H (2007). Autoreactivity in human IgG+ memory B cells. Immunity 26, 205–213. [PubMed: 17306569]

Trapecar M, Khan S, Roan NR, Chen T-H, Telwatte S, Deswal M, Pao M, Somsouk M, Deeks SG, Hunt PW, et al. (2017). An optimized and validated method for isolation and characterization of lymphocytes from HIV+ human gut biopsies. AIDS Res. Hum. Retroviruses 33 (S1), S31–S39. [PubMed: 28882052]

Turner RB (2007). Rhinovirus: more than just a common cold virus. J. Infect. Dis 195, 765–766. [PubMed: 17299703]

Turner RB, Weingand KW, Yeh C-H, and Leedy DW (1998). Association between interleukin-8 concentration in nasal secretions and severity of symptoms of experimental rhinovirus colds. Clin. Infect. Dis 26, 840–846. [PubMed: 9564459]

Turner RB, Woodfolk JA, Borish L, Steinke JW, Patrie JT, Muehling LM, Lahtinen S, and Lehtinen MJ (2017). Effect of probiotic on innate inflammatory response and viral shedding in experimental rhinovirus infection - a randomised controlled trial. Benef. Microbes 8, 207–215. [PubMed: 28343401]

van der Maaten L, and Hinton G (2008). Visualizing data using t-SNE. J. Mach. Learn. Res 9, 2579–2605.

Van Gassen S, Callebaut B, Van Helden MJ, Lambrecht BN, Demeester P, Dhaene T, and Saeys Y (2015). FlowSOM: Using self-organizing maps for visualization and interpretation of cytometry data. Cytometry A 87, 636–645. [PubMed: 25573116]

Wang S, Wang J, Kumar V, Karnell JL, Naiman B, Gross PS, Rahman S, Zerrouki K, Hanna R, Morehouse C, et al.; Autoimmunity Molecular Medicine Team (2018). IL-21 drives expansion and plasma cell differentiation of autoreactive CD11chiT-bet+ B cells in SLE. Nat. Commun 9, 1758. [PubMed: 29717110]

Wardemann H, Yurasov S, Schaefer A, Young JW, Meffre E, and Nussenzweig MC (2003). Predominant autoantibody production by early human B cell precursors. Science 301, 1374–1377. [PubMed: 12920303]

Weber LM, and Robinson MD (2016). Comparison of clustering methods for high-dimensional single-cell flow and mass cytometry data. Cytometry A 89, 1084–1096. [PubMed: 27992111]

Weiss GE, Crompton PD, Li S, Walsh LA, Moir S, Traore B, Kayentao K, Ongoiba A, Doumbo OK, and Pierce SK (2009). Atypical memory B cells are greatly expanded in individuals living in a malaria-endemic area. J. Immunol 183, 2176–2182. [PubMed: 19592645]

Wilkerson MD, and Hayes DN (2010). ConsensusClusterPlus: a class discovery tool with confidence assessments and item tracking. Bioinformatics 26, 1572–1573. [PubMed: 20427518]

Zambrano JC, Carper HT, Rakes GP, Patrie J, Murphy DD, Platts-Mills TAE, Hayden FG, Gwaltney JM Jr., Hatley TK, Owens AM, and Heymann PW (2003). Experimental rhinovirus challenges in adults with mild asthma: response to infection in relation to IgE. J. Allergy Clin. Immunol 111, 1008–1016. [PubMed: 12743565]

Zunder ER, Finck R, Behbehani GK, Amir AD, Krishnaswamy S, Gonzalez VD, Lorang CG, Bjornson Z, Spitzer MH, Bodenmiller B, et al. (2015). Palladium-based mass tag cell barcoding with a doublet-filtering scheme and single-cell deconvolution algorithm. Nat. Protoc 10, 316–333. [PubMed: 25612231]

Author Manuscript Author Manuscript Author Manuscript Author Manuscript

Highlights

- Distinct memory B cells mediate local and systemic responses to rhinovirus
- CXCR5-T-bet+ B cells link to acute cross-reactive IgG secretion in the nose
- CXCR5+ B cells link to strain-specific antibody isotypes found later in serum
- CXCR5− and CXCR5+ B cell subsets are clonally distinct

Author Manuscript Author Manuscript Author Manuscript Author Manuscript

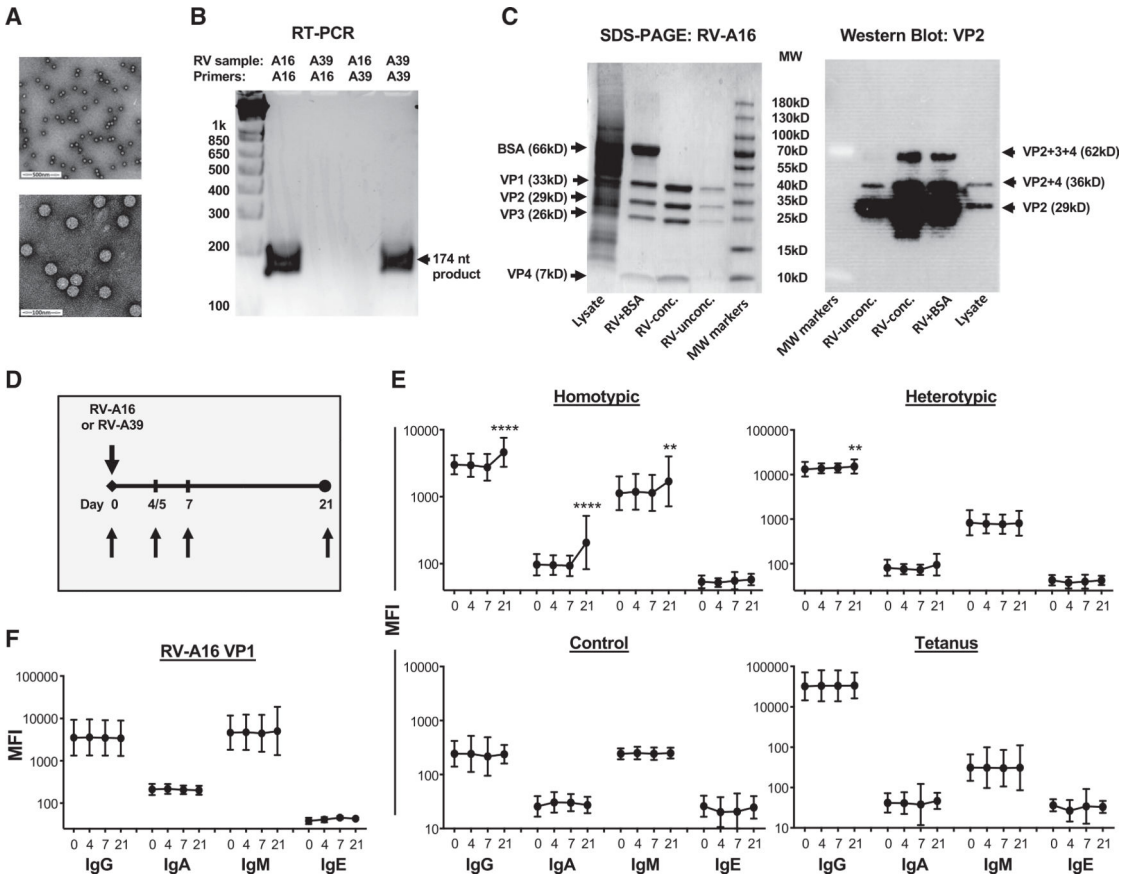

Figure 1. Whole Virus Detects Multiple RV-Specific Isotypes

(A-C) Purification of whole virus.

(A) Purified RV by electron microscopy at low (12,000×) and high (60,000×) magnification. Scale bars denote 500 and 100 nm, respectively.

(B) PCR analysis of strains RV-A16 and RV-A39 using strain-specific primers.

(C) SDS-PAGE analysis with silver staining of RV-A16 and corresponding western blot for VP2. RV was purified from cell lysates prepared in buffer with 0.01% BSA for virus stability and subsequently isolated in pure PBS. RV preparations were analyzed before (RV-unconc.) or after (RV-conc.) concentration to confirm purity. The identity of RV-A16 was confirmed by western blot using anti-VP2 mAb. Higher molecular weight immature polyproteins containing uncleaved VP2 are denoted. Similar results were obtained for RV-A39.

(D) Model of experimental RV infection in humans. Arrows denote time points for blood draws. Blood was available on day 7 only for subjects challenged with RV-A16.

(E) Longitudinal analysis of serum antibodies specific for homotypic or heterotypic whole virus (depending on infecting strain) at days 0, 4/5, 7, and 21 after RV inoculation (13 subjects infected with RV-A16 and 12 subjects infected with RV-A39; n = 25 for all time points, except for day 7 [n = 13]).

(F) Longitudinal analysis of serum antibodies specific for RV-A16 VP1 in 13 subjects infected with RV-A16.

Author Manuscript Author Manuscript Author Manuscript Author Manuscript

Significance was determined by Wilcoxon matched pairs signed-rank test (E and F). Geometric mean ± geometric SD. **p < 0.01 and ****p < 0.0001 versus day 0. See also Figure S1.

Author Manuscript Author Manuscript Author Manuscript Author Manuscript

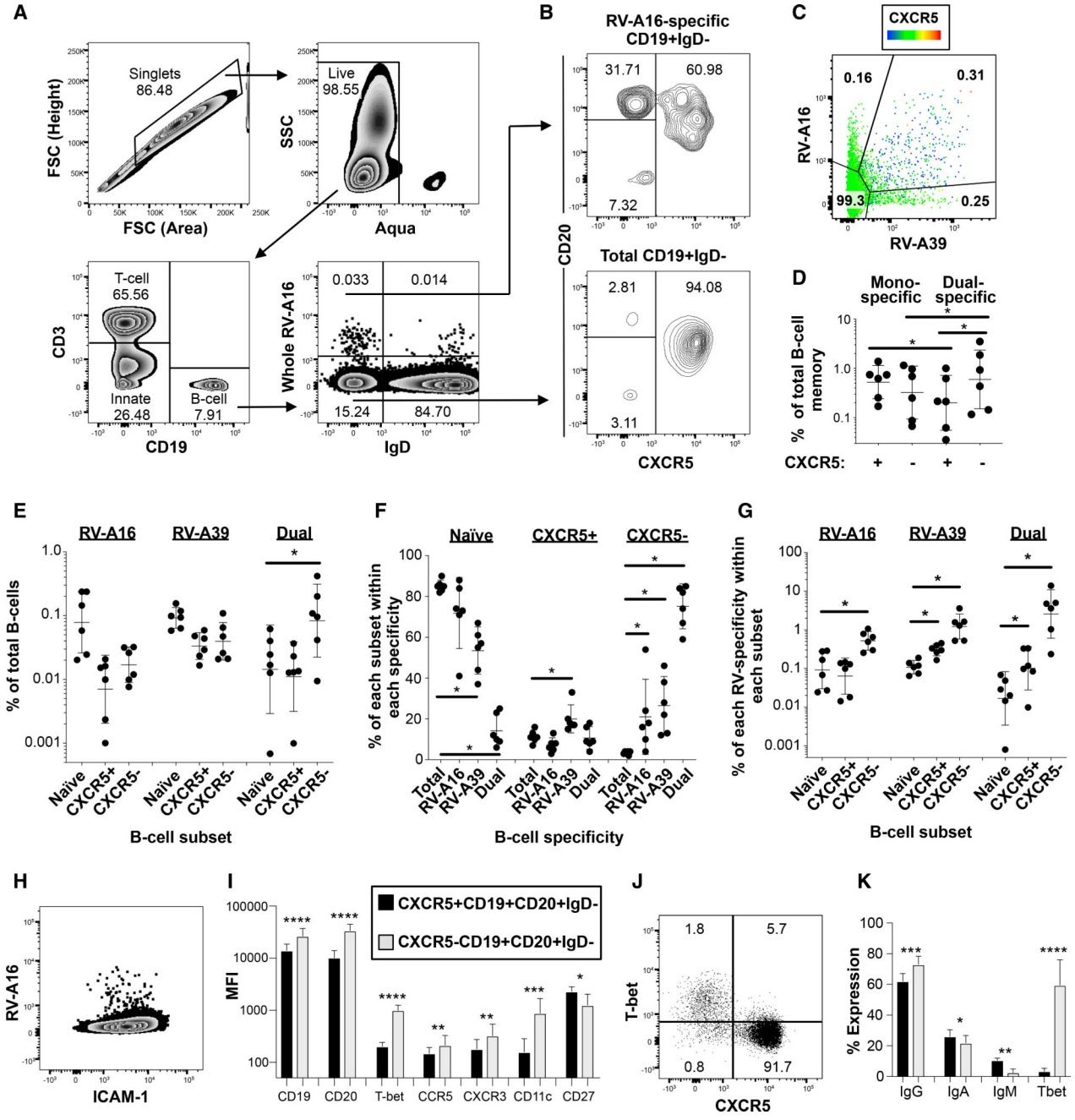

Figure 2. Dual-Specific B Cells Are Expanded in the Blood and Lack CXCR5

(A) Gating strategy for virus-specific B cells showing their enrichment within the IgD-negative subset.

(B) Comparison of the percentages of CXCR5+ and CXCR5− cells within virus-specific and total memory B cells.

(C) Total B cells stained for RV-A16 and RV-A39 and colored for CXCR5 expression. Data in (A)-(C) are representative of six subjects.

(D) Percentages of CXCR5+ and CXCR5− mono-specific and dual-specific B cells within total memory B cells (CD19+CD20+IgD−) (n = 6).

Author Manuscript Author Manuscript Author Manuscript Author Manuscript

(E) The percentage of each RV specificity within total B cells according to naive (IgD+) and memory (CXCR5+ or CXCR5−) phenotype (n = 6).
(F) The percentage of naive, CXCR5+ memory, and CXCR5− memory B cells within RV-specific B cells (n = 6).
(G) The percentage of mono-specific and dual-specific B cells within naive, CXCR5+ memory, and CXCR5− memory B cell subsets (n = 6).
(H) Total B cells stained for RV-A16 and ICAM-1 without ICAM-1 blocking.
(I) Comparison of cell marker MFI of CXCR5+ and CXCR5− memory subsets (n = 8).
(J) Representative scatterplot of memory B cells analyzed for T-bet and CXCR5 expression.
(K) Comparison of isotype and T-bet expression in CXCR5+ and CXCR5− memory subsets (n = 8).
Significance was determined by Wilcoxon matched pairs signed-rank test (D, E, F, G, I, and K). Geometric mean ± geometric SD (D, E, G, and I). Mean ± SD (F and K). *$p < 0.05$, **$p < 0.01$, ***$p < 0.001$, and ****$p < 0.0001$.

Author Manuscript Author Manuscript Author Manuscript Author Manuscript

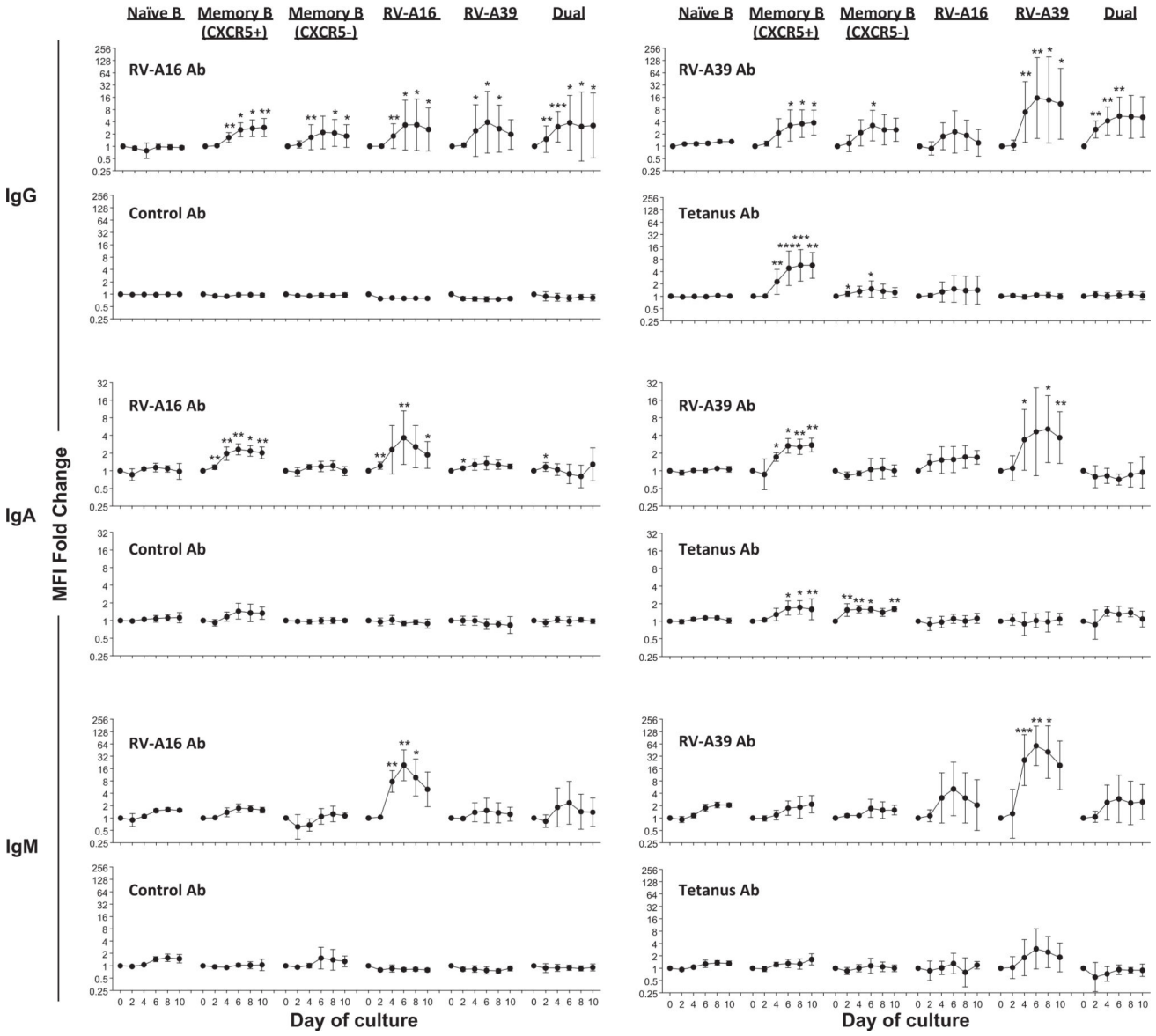

Figure 3. Dual-Specific B Cells Rapidly Secrete Cross-Reactive IgG but Not IgA or IgM

Purified B cell types were cultured for 10 days under plasma cell differentiating conditions and secretion of antibody isotypes was assessed every 2 days. Data are shown for the change over baseline in specific antibodies for RV-A16, RV-A39, tetanus toxin C-terminal fragment, and mouse IgG (control) (n = 6 subjects). Significance was determined by Friedman multiple comparisons test. Geometric mean ± geometric SD. *$p < 0.05$, **$p < 0.01$, ***$p < 0.001$, and ****$p < 0.0001$ versus day 0.

See also Figure S2.

Author Manuscript Author Manuscript Author Manuscript Author Manuscript

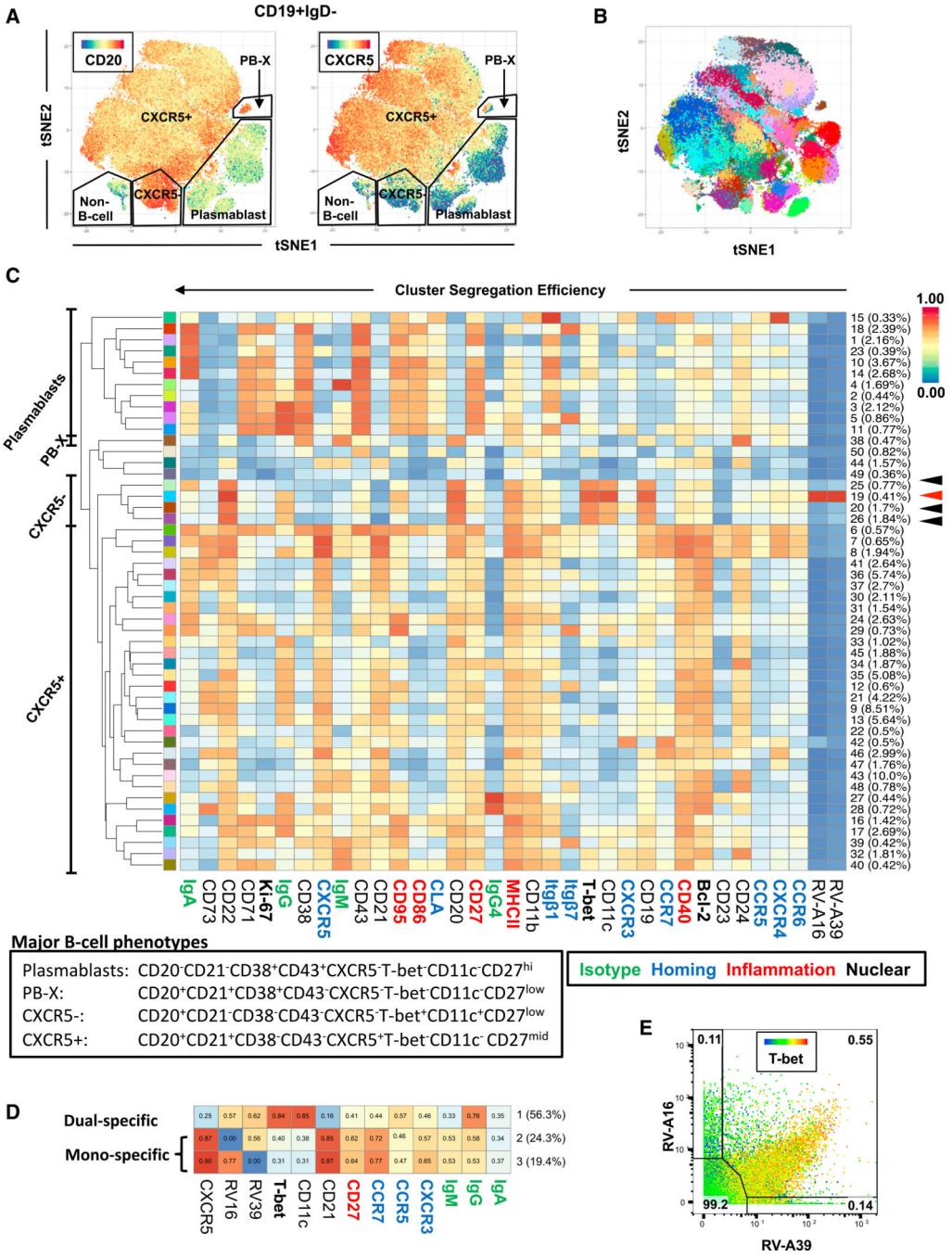

Figure 4. High-Dimensional Analysis Reveals a Characteristic Signature of Dual-Specific B Cells

B cells were analyzed by mass cytometry during experimental infection, and data were pooled from 70 samples analyzed from 24 subjects challenged with either RV-A16 (n = 13) or RV-A39 (n = 11).

(A) t-SNE distribution for total memory B cells and plasmablasts (CD19+ IgD− cells) colorized by CD20 expression (plasmablasts [low], CXCR5+ memory [mid], and CXCR5− memory [high]) and CXCR5 expression (plasmablasts [low], CXCR5+ memory [high], and CXCR5− memory [low]).

Author Manuscript Author Manuscript Author Manuscript Author Manuscript

(B) Total memory B cells and plasmablasts clustered into 50 phenotypes overlaid on t-SNE map.
(C) Heatmap of all phenotypes according to expression of all markers assessed by the FlowSOM algorithm. B cell types are denoted on the left side, and colors in the left column correspond to each of the 50 cluster phenotypes in (B). Numbers listed on the right denote the number assigned to each cluster and average percentages. Arrowheads denote CXCR5− memory B cell clusters that include a subset dual-specific for RV-A strains (cluster 19). Major differentiating markers for plasmablasts, PB-X, CXCR5− memory, and CXCR5+ memory types shown in the heatmap are summarized in the table.
(D) Comparison of dual-specific and mono-specific phenotypes within total RV-specific memory B cells, showing only those markers used in multi-color flow cytometry.
(E) Pooled total B cells stained for RV-A16 and RV-A39, and colored for T-bet expression.

Author Manuscript Author Manuscript Author Manuscript Author Manuscript

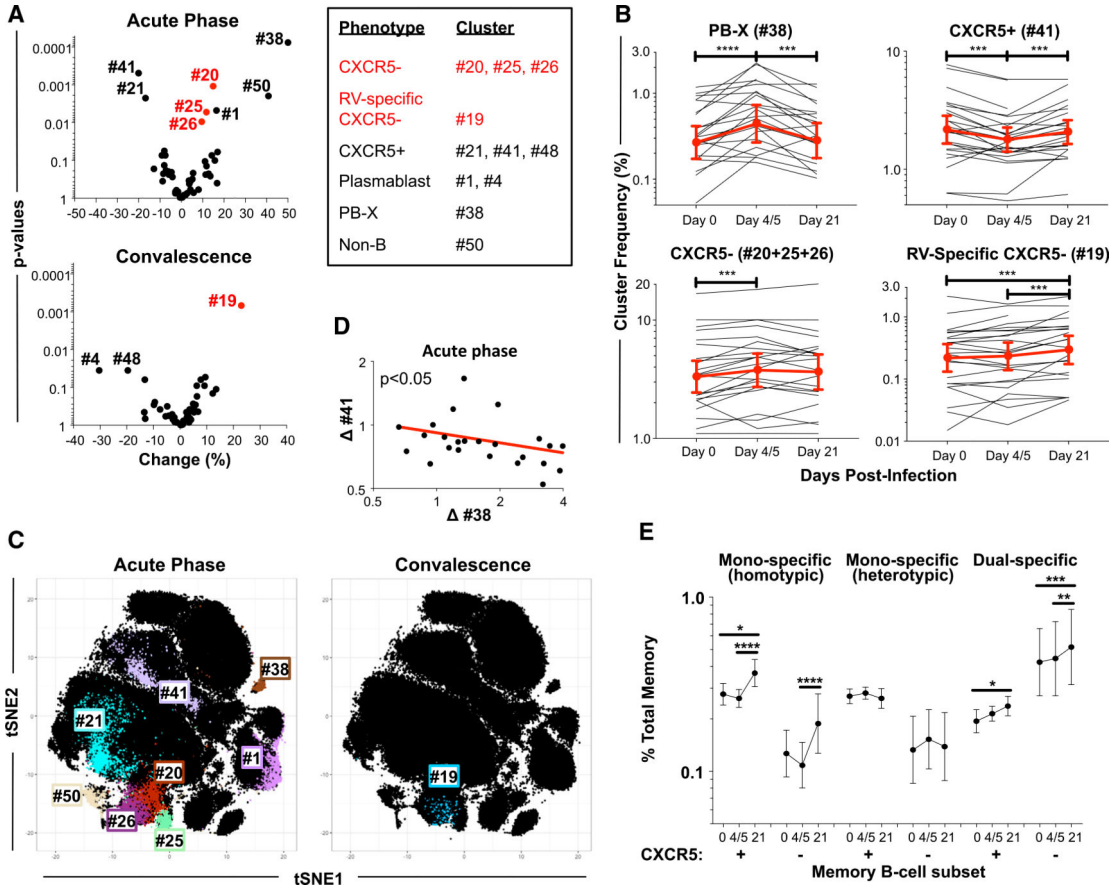

Figure 5. Dual-Specific B Cells Expand after Rhinovirus Infection

(A) Volcano plots showing p values for percentage changes of clusters within CD19+IgD− cells (see Figure 4C for designated cluster number) during acute infection (day 4/5, n = 24) and convalescence (day 21, n = 22).

(B) Change in the percentage of B cell clusters during the course of infection for each subject.

(C) t-SNE maps for CD19+IgD− cells (corresponding to Figure 4A, but shown in black) with overlay of B cell clusters that changed significantly ($p < 0.01$) during the acute phase (left panel) and convalescence (right panel). Colors of cell clusters correspond to cluster phenotypes in Figure 4B.

(D) Correlation between the change in PB-X (cluster 38) and CXCR5+ memory B cells (cluster 41) during the acute phase (n = 24).

(E) Change in the percentages of CXCR5+ and CXCR5− mono-specific and dual-specific memory B cells during RV infection, determined by manual gating (n = 24). Mono-specific B cells were analyzed in relation to challenge with homotypic and heterotypic RV-A strains. Significance was determined by Wilcoxon matched pairs signed-rank test (A, B, and E) and Spearman correlation (D). Geometric mean ± geometric SD (B and E).

*$p < 0.05$, **$p < 0.01$, ***$p < 0.001$, and ****$p < 0.0001$.

See also Figure S3.

Author Manuscript Author Manuscript Author Manuscript Author Manuscript

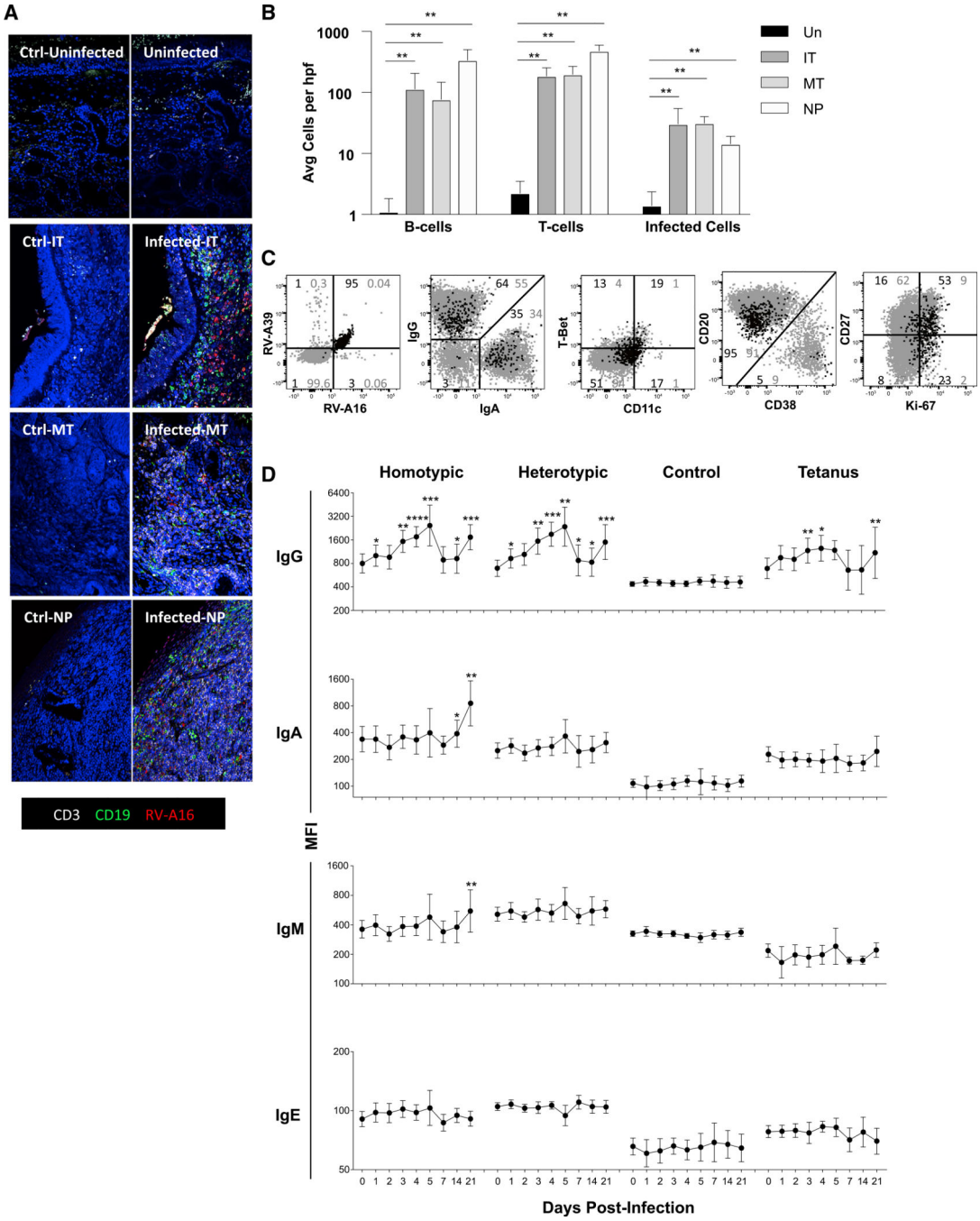

Figure 6. Early Antibody Responses to RV in the Nose Are Cross-Reactive, Limited to IgG, and Coincide with Infiltrating Dual-Specific B Cells

(A) Immunohistochemistry analysis of nasal tissue analyzed for CD19 (green), CD3 (white), RV (red), and DNA (blue). Panels on the right show tissue from an uninfected subject (top) and from an infected subject at inferior turbinate (IT), middle turbinate (MT), and nasopharyngeal (NP) sites. Left panels show corresponding negative controls (Ctrl) prepared without primary antibodies. Data are representative of five subjects infected with RV-A16. (B) Cell counts in nasal biopsies from infected subjects after RV-A16 challenge and in uninfected (Un) controls (five per group). Specimens from uninfected subjects were

Author Manuscript Author Manuscript Author Manuscript Author Manuscript

available for a single nasal site only. Averages for each subject were calculated from four image locations within each biopsy.

(C) Scatter plots of B cells isolated from nasal tissue (inferior turbinate) from a subject infected with RV-A16 at day 4. Memory B cells (CD19+IgD−) in the nose (black) are overlaid on memory B cells (gray) from the blood of a healthy control for comparison. Representative of three infected subjects.

(D) Longitudinal analysis of antibody isotypes specific for homotypic or heterotypic virus (depending on infecting strain) in nasal washes during RV infection (subjects infected with RV-A16 and RV-A39 = 13 and 12, respectively; n = 25 for all time points).

Significance was determined by Mann Whitney ranked-sum test (B) or Wilcoxon matched pairs signed-rank test (D). Geometric mean ± geometric SD (B and D).

*$p < 0.05$, **$p < 0.01$, ***$p < 0.001$, and ****$p < 0.0001$ versus uninfected tissue (B) or day 0 (D).

See also Figures S4, S5, and S6.

Author Manuscript Author Manuscript Author Manuscript Author Manuscript

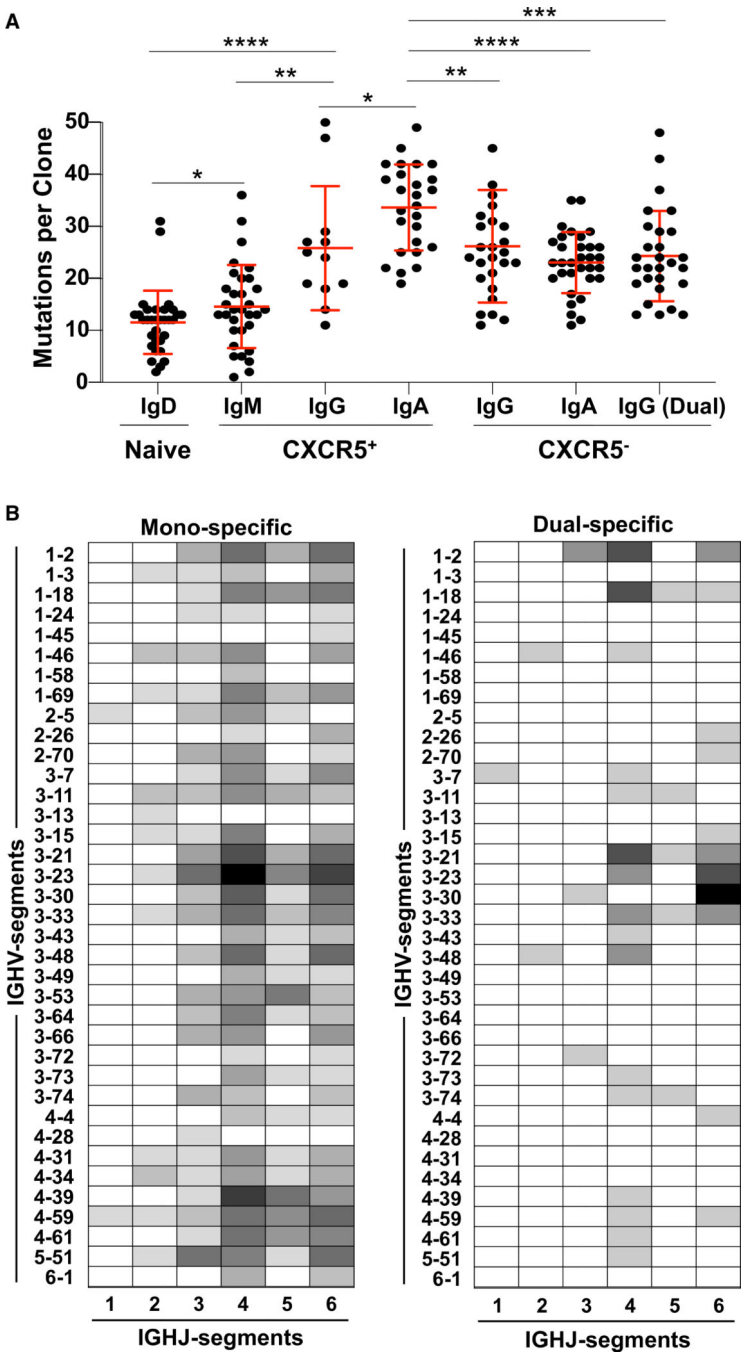

Figure 7. Dual-Specific B Cells Are Clonally Distinct from Their Mono-specific Counterparts

(A) Somatic hypermutation counts at immunoglobulin heavy chain loci in sorted RV-specific single B cells. Dual-specific B cells were sorted as a separate phenotype for CXCR5− IgG+ cells only.

(B) VDJ segment usage in mono-specific and dual-specific B cells (114 and 57 cells, respectively).

Significance was determined by Mann-Whitney ranked-sum test (A). Mean ± SD. *$p < 0.05$, **$p < 0.01$, ***$p < 0.001$, and ****$p < 0.0001$.

Author Manuscript Author Manuscript Author Manuscript Author Manuscript

See also Figure S2.

Author Manuscript Author Manuscript Author Manuscript Author Manuscript

KEY RESOURCES TABLE

REAGENT or RESOURCE	SOURCE	IDENTIFIER
Antibodies		
Anti-human beta 2 microglobulin (CyTOF)	BioLegend	Cat#316302; RRID:AB_492835
Anti-Bcl-2 (CyTOF)	BioLegend	Cat#658702; RRID:AB_2562959
Anti-human CCR5-144Nd (CyTOF)	Fluidigm	Cat#3144007A
Anti-human CCR5-PE (FC)	ThermoFisher	Cat#12-1956-42; RRID:AB_2572593
Anti-human CCR6 (CyTOF)	BioLegend	Cat#353402; RRID:AB_10918625
Anti-human CCR7 (CyTOF)	Fluidigm	Cat#3159003; RRID:AB_2714155
Anti-human CD11b (CyTOF)	Fluidigm	Cat#3209003; RRID:AB_2687654
Anti-human CD11c (CyTOF, FC)	BioLegend	Cat#301602; RRID:AB_314172
Anti-human CD11c (FC)	BioLegend	Cat#301605; RRID:AB_314175
Anti-human CD11c (IHC)	Abcam	Cat#ab52632; RRID:AB_2129793
Anti-human CD123 (CyTOF)	BioLegend	Cat# 306002; RRID:AB_2661822
Anti-human CD123 MicroBeads	Miltenyi Biotec	Cat#130-094-432
Anti-human CD14 (CyTOF)	BioLegend	Cat#301802; RRID:AB_314184
Anti-human CD14 MicroBeads	Miltenyi Biotec	Cat#130-097-052
Anti-human CD16 (CyTOF)	BioLegend	Cat#302002; RRID:AB_314202
Anti-human CD16 MicroBeads	Miltenyi Biotec	Cat#130-094-432
Anti-human CD19-142Nd (CyTOF)	Fluidigm	Cat#3142001; RRID:AB_2651155
Anti-human CD19-PE-Cy7 (FC)	BioLegend	Cat#302216; RRID:AB_314246
Anti-human CD19 (IHC)	ThermoFisher	Cat#14-019-482; RRID:AB_2637171
Anti-human CD20 (CyTOF)	BioLegend	Cat#302302; RRID:AB_314250
Anti-human CD20-Brilliant Violet 711 (FC)	BioLegend	Cat#302342; RRID:AB_2562602
Anti-human CD20 (IHC)	BioPrime	Cat#BC500
Anti-human CD21 (CyTOF)	Fluidigm	Cat#3152010B
Anti-human CD22 (CyTOF)	BioLegend	Cat#302502; RRID:AB_314264
Anti-human CD23 (CyTOF)	BioLegend	Cat#338502; RID:AB_1279181
Anti-human CD235a (CyTOF)	BioLegend	Cat#306602; RRID:AB_314620
Anti-human CD235a MicroBeads	Miltenyi Biotec	Cat#130-050-501
Anti-human CD24 (CyTOF)	BioLegend	Cat#311102; RRID:AB_314851
Anti-human CD27 (CyTOF)	BioLegend	Cat#302802; RRID:AB_314294
Anti-human CD27-PE-Cy5 (FC)	ThermoFisher	Cat#15-0279-41; RRID:AB_10717248
Anti-human CD3-170Er (CyTOF)	Fluidigm	Cat#3170001B; RRID:AB_2811085
Anti-human CD3-PerCP (FC)	BioLegend	Cat#344814; RRID:AB_10639948
Anti-human CD3e (IHC)	ThermoFisher	Cat# MA5-14524; rRID:AB_10982026
Anti-human CD3 MicroBeads	Miltenyi Biotec	Cat#130-097-043
Anti-human CD38 (CyTOF)	BioLegend	Cat#303502; RRID:AB_314354
Anti-human CD38 (FC)	BD Biosciences	Cat#564979; RRID:AB_2744373
Anti-human CD40 (CyTOF)	BioLegend	Cat#334302; RRID:AB_1236384

Author Manuscript Author Manuscript Author Manuscript Author Manuscript

REAGENT or RESOURCE	SOURCE	IDENTIFIER
Anti-human CD40 (for *in vitro* stimulation)	BioLegend	Cat#313009; RRID:AB_314972
Anti-human CD43 (CyTOF)	BioLegend	Cat#343202; RRID:AB_1659198
Anti-human CD45 (CyTOF)	BioLegend	Cat#304002; RRID:AB_314390
Anti-human CD45 (CyTOF)	BioLegend	Cat#361902; RRID:AB_2563177
Anti-human CD71 (CyTOF)	BioLegend	Cat#334102; RRID:AB_1134247
Anti-human CD73-168Er (CyTOF)	Fluidigm	Cat#3168015B; RRID:AB_2810249
Anti-human CD86 (CyTOF)	BioLegend	Cat#305402; RRID:AB_314522
Anti-human CD95 (CyTOF)	BioLegend	Cat#305602; RRID:AB_314540
Anti-human CLA (CyTOF)	BioLegend	Cat#321302; RRID:AB_492894
Anti-human CXCR3 (CyTOF)	BioLegend	Cat#353702; RRID: AB_10983073
Anti-human CXCR3-PE/Dazzle 594 (FC)	BioLegend	Cat#353735; RRID:AB_2564287
Anti-human CXCR4 (CyTOF)	BioLegend	Cat#306502; RRID: AB_314608
Anti-human CXCR5 (CyTOF)	BioLegend	Cat#356902; RRID:AB_2561811
Anti-human CXCR5-Brilliant Violet 421 (FC)	BioLegend	Cat#356920; RRID:AB_2562303
Donkey anti-Mouse IgG (IHC)	ThermoFisher	Cat#A16019; RRID:AB_2534693
Donkey anti-Rabbit IgG (IHC)	ThermoFisher	Cat#A16037; RRID:AB_2534711
Donkey anti-Rat IgG (IHC)	ThermoFisher	Cat#A18747; RRID:AB_2535524
Anti-human FcεRI (CyTOF)	BioLegend	Cat#334602; RRID:AB_1227649
Anti-human ICAM-1 (Block, FC)	BioLegend	Cat#322704; RRID:AB_535976
Anti-human IgA (CyTOF)	Miltenyi Biotec	Cat#130-093-073; RRID:AB_1036150
Anti-human IgA-APC-Vio770 (FC)	Miltenyi Biotec	Cat#130-107-052; RRID:AB_2659727
Anti-human IgA-PE-Vio770 (Multiplex)	Miltenyi Biotec	Cat#130-107-077; RRID:AB_2659724
Anti-human IgD (CyTOF)	BioLegend	Cat#348202; RRID:AB_10550095
Anti-human IgD-PerCP-eFluor710 (FC)	ThermoFisher	Cat#46-9868-42; RRID: AB_2573920
Anti-human IgE (CyTOF)	BioLegend	Cat#325502; RRID:AB_830847
Anti-human IgE-APC (FC)	BioLegend	Cat#325507; RRID:AB_10897941
Anti-human IgE (Multiplex)	BD Biosciences	Cat#745980; RRID:AB_2743386
Anti-human IgG (CyTOF, Multiplex)	BD Biosciences	Cat#555784; RRID:AB_396119
Anti-human IgG (FC)	BD Biosciences	Cat#564230; RRID:AB_2738684
Anti-human IgM-172Yb (CyTOF)	Fluidigm	Cat#3172004B; RRID:AB_2810858
Anti-human IgM-Brilliant Violet 650 (FC)	BioLegend	Cat#314525; RRID:AB_2563382
Anti-human IgM (Multiplex)	BioLegend	Cat#314502; RRID:AB_493003
Anti-human integrin β1 (CyTOF)	BioLegend	Cat#303002; RRID:AB_314318
Anti-human/mouse integrin β7 (CyTOF)	BioLegend	Cat#321202; RRID:AB_571975
Anti-human Ki-67 (CyTOF, FC)	BioLegend	Cat#350502; RRID:AB_10662385
Anti-human HLA-A, B, C (MHCI) (CyTOF)	BioLegend	Cat#311402; RRID:AB_314871
Anti-human HLA-DR, DP, DQ (MHCII) (CyTOF)	BioLegend	Cat#361702; RRID:AB_2563139
mIgG4 (CyTOF)	Sanquin	Gift of T. Rispens
Anti-RV-A16 VP2 (IHC)	QED Bioscience	Cat#18758

Author Manuscript Author Manuscript Author Manuscript Author Manuscript

REAGENT or RESOURCE	SOURCE	IDENTIFIER
Anti-human IgG4 (CyTOF)	BD Biosciences	Cat# 555881; RRID:AB_396193
Anti-human/mouse T-bet (CyTOF, IHC)	BioLegend	Cat#644802; RRID:AB_1595503
Anti-human/mouse T-bet-Brilliant Violet 605 (FC)	BioLegend	Cat#644817; RRID:AB_11219388
Bacterial and Virus Strains		
RV-A16 challenge pool	UVA	N/A
RV-A39 challenge pool	UVA	N/A
Biological Samples		
PBMCs from healthy and RV infected adults	This paper	N/A
Nasal biopsy tissue from healthy and RV infected adults	This paper	N/A
Serum from healthy and RV infected adults	This paper	N/A
Chemicals, Peptides, and Recombinant Proteins		
Benzonase	Millipore	Cat#1016970001
CpG DNA ODN-2006 (Stimulation)	Miltenyi Biotec	Cat#130-100-106
CTL Wash	Immunospot	Cat#CTLW-010
DNase I	SigmaAldrich	Cat#D5025-15KU
Fetal Bovine Serum	ThermoFisher	Cat#16000044
FoxP3 Fix/Perm	ThermoFisher	Cat#00-5523-00
Human IL-10 (Stimulation)	Miltenyi Biotec	Cat#130-093-947
Human IL-2 (Stimulation)	Miltenyi Biotec	Cat#130-097-742
Human IL-21 (Stimulation)	Miltenyi Biotec	Cat#130-094-563
IMDM	ThermoFisher	Cat#12-440-053
Insulin/transferrin/selenium	ThermoFisher	Cat#41400045
Liberase TM	SigmaAldrich	Cat#5401119001
MEM	ThermoFisher	Cat#11-090-073
Non-Essential Amino Acids	ThermoFisher	Cat# 11-140-050
Pluronic	ThermoFisher	Cat#24-040-032
RPMI-1640	ThermoFisher	Cat#11875093
RV-A16 VP1	MedUni Wien	Gift of R. Valenta
S-MEM	ThermoFisher	Cat#11-380-037
Tetanus Toxin c-Terminal Fragment	TechLab	Gift of J. Herbein
Critical Commercial Assays		
BCA Protein Quantification	ThermoFisher	Cat#23227
BCR Next-Generation Sequencing	Illumina	MiSeq
Human BCR Single Cell mRNA Barcoding	10x Genomics	Chromium Controller
Deposited Data		
RNA seq data	This paper	NCBI SRA: PRJNA580187
Experimental Models: Cell Lines		
HeLa H1 Cells	ATCC	Cat#CRL-1958
Oligonucleotides		

Author Manuscript Author Manuscript Author Manuscript Author Manuscript

REAGENT or RESOURCE	SOURCE	IDENTIFIER
Primer Pan RV FW: CCTCCGGCCCCTGAA	Turner et al., 2017	N/A
Primer Pan RV RV: AAACACGGACACCCAAAGTAG	Turner et al., 2017	N/A
Primer RV-A16 FW: CATGAATCAGTGTTGGATATTGTGGAC	This paper	N/A
Primer RV-A16 RV: AATGTGACCATCTTTGGCTGCTAC	This paper	N/A
Primer RV-A39 FW: CACATTTCCACAATTACTATGAAGAAGGAG	This paper	N/A
Primer RV-A39 RV: ATCTTCACCTCTTCCAGCTATGCA	This paper	N/A
Software and Algorithms		
Cell Ranger	10x Genomics	https://support.10xgenomics.com
ConsensusClusterPlus	Wilkerson and Hayes, 2010	http://bioconductor.org/packages/release/bioc/html/ConsensusClusterPlus.html
CyTOF Data Normalizer	Fluidigm	https://fluidigm.com/documents
CyTOF Debarcoder	Zunder et al., 2015	https://github.com/zunderlab
Flowjo	TreeStar	https://flowjo.com
FlowSOM	Van Gassen et al., 2015	http://bioconductor.org/packages/release/bioc/html/FlowSOM.html
Loupe VDJ Browser	10x Genomics	https://support.10xgenomics.com
MATLAB	MathWorks	https://www.mathworks.com/products/matlab.html
RStudio	RStudio	https://rstudio.com
t-SNE	van der Maaten and Hinton, 2008	http://lvdmaaten.github.io/tsne/
Zen Microscopy Imaging	Zeiss	https://zeiss.com/microscopy/us/products/microscope-software/zen.html
Other		
AlexaFluor 405 Conjugation (Multiplex)	ThermoFisher	Cat#A30000
AlexaFluor 488 Conjugation (FC, Multiplex)	ThermoFisher	Cat#A30052
AlexaFluor 568 Conjugation (FC)	ThermoFisher	Cat#A20003
AlexaFluor 647 Conjugation (Multiplex)	ThermoFisher	Cat#A20006
Cisplatin Pt194 (CyTOF)	Fluidigm	Cat#201194
Cisplatin Pt198 (CyTOF)	Fluidigm	Cat#201198
DAPI (IHC)	PromoKine	Cat#PK-CA707-40043
Fixable Viability Stain 510 (Multiplex)	Becton Dickinson	Cat#564406
DNA Intercalator-Ir193 (CyTOF)	Fluidigm	Cat#201192B
DNA Intercalator-Rh103 (CyTOF)	Fluidigm	Cat#201103B
Isothiocyanobenzyl-EDTA	Dojindo	Cat#M030-10
Live/Dead Aqua (FC)	ThermoFisher	Cat#L34966

Author Manuscript Author Manuscript Author Manuscript Author Manuscript

REAGENT or RESOURCE	SOURCE	IDENTIFIER
Metal-Antibody Conjugation Pr141 (CyTOF)	Fluidigm	Cat#201141A
Metal-Antibody Conjugation Nd143 (CyTOF)	Fluidigm	Cat#201143A
Metal-Antibody Conjugation Nd145 (CyTOF)	Fluidigm	Cat#201145A
Metal-Antibody Conjugation Nd146 (CyTOF)	Fluidigm	Cat#201146A
Metal-Antibody Conjugation Sm147 (CyTOF)	Fluidigm	Cat#201147A
Metal-Antibody Conjugation Nd148 (CyTOF)	Fluidigm	Cat#201148A
Metal-Antibody Conjugation Sm149 (CyTOF)	Fluidigm	Cat#201149A
Metal-Antibody Conjugation Nd150 (CyTOF)	Fluidigm	Cat#201150A
Metal-Antibody Conjugation Eu151 (CyTOF)	Fluidigm	Cat#201151A
Metal-Antibody Conjugation Eu153 (CyTOF)	Fluidigm	Cat#201141A
Metal-Antibody Conjugation Sm154 (CyTOF)	Fluidigm	Cat#201154A
Metal-Antibody Conjugation Gd155 (CyTOF)	Fluidigm	Cat#201155A
Metal-Antibody Conjugation Gd156 (CyTOF)	Fluidigm	Cat#201156A
Metal-Antibody Conjugation Gd158 (CyTOF)	Fluidigm	Cat#201158A
Metal-Antibody Conjugation Gd160 (CyTOF)	Fluidigm	Cat#201160A
Metal-Antibody Conjugation Dy161 (CyTOF)	Fluidigm	Cat#201161A
Metal-Antibody Conjugation Dy162 (CyTOF)	Fluidigm	Cat#201162A
Metal-Antibody Conjugation Dy163 (CyTOF)	Fluidigm	Cat#201163A
Metal-Antibody Conjugation Dy164 (CyTOF)	Fluidigm	Cat#201164A
Metal-Antibody Conjugation Ho165 (CyTOF)	Fluidigm	Cat#201165A
Metal-Antibody Conjugation Er166 (CyTOF)	Fluidigm	Cat#201166A
Metal-Antibody Conjugation Er167 (CyTOF)	Fluidigm	Cat#201167A
Metal-Antibody Conjugation Tm169 (CyTOF)	Fluidigm	Cat#201169A
Metal-Antibody Conjugation Er170 (CyTOF)	Fluidigm	Cat#201170A
Metal-Antibody Conjugation Yb171 (CyTOF)	Fluidigm	Cat#201171A
Metal-Antibody Conjugation Yb173 (CyTOF)	Fluidigm	Cat#201173A
Metal-Antibody Conjugation Yb174 (CyTOF)	Fluidigm	Cat#201174A
Metal-Antibody Conjugation Lu175 (CyTOF)	Fluidigm	Cat#201175A
Metal-Antibody Conjugation Yb176 (CyTOF)	Fluidigm	Cat#201176A
Osmium 190 (CyTOF)	TraceSciences.com	Cat#Os-190
Osmium 192 (CyTOF)	TraceSciences.com	Cat#Os-192
Palladium 102 (CyTOF)	BuyIsotope.com	Cat#Pd-102
Palladium 104 (CyTOF)	BuyIsotope.com	Cat#Pd-104
Palladium 105 (CyTOF)	BuyIsotope.com	Cat#Pd-105
Palladium 106 (CyTOF)	BuyIsotope.com	Cat#Pd-106
Palladium 108 (CyTOF)	BuyIsotope.com	Cat#Pd-108
Palladium 110 (CyTOF)	BuyIsotope.com	Cat#Pd-110
Sulfo-NHS-LC-Biotin Conjugation (Multiplex)	ThermoFisher	Cat#21335

REAGENT or RESOURCE	SOURCE	IDENTIFIER
Tetramethylrhodamine Conjugation (IHC)	ThermoFisher	Cat#46406

Author Manuscript Author Manuscript Author Manuscript Author Manuscript